EVALUATING SHRUB EXPANSION IN A SUBARCTIC MOUNTAIN BASIN USING MULTI-TEMPORAL LIDAR DATA

EVALUATING SHRUB EXPANSION IN A SUBARCTIC MOUNTAIN BASIN USING MULTI-TEMPORAL LIDAR DATA

By SEAN C. LEIPE, B.Sc.

A Thesis Submitted to the School of Graduate Studies in Partial Fulfillment of the Requirements for the Degree Master of Science

McMaster University

MASTER OF SCIENCE (2020) MCMASTER UNIVERSITY

EARTH, ENVIRONMENT, & SOCIETY HAMILTON, ONTARIO

TITLE: Evaluating shrub expansion in a subarctic mountain basin using multi-temporal LiDAR data

AUTHOR: Sean C. Leipe, B.Sc – Earth and Environmental Science (McMaster University)

SUPERVISOR: Dr. Sean K. Carey

NUMBER OF PAGES: vii, 62

ABSTRACT

High-latitude ecosystems have experienced substantial warming over the past 40 years, which is expected to continue into the foreseeable future. Consequently, an increase in vegetation growth has occurred throughout the circumpolar North as documented through remote sensing and plot-level studies. A major component of this change is shrub expansion (shrubbing) in arctic and subarctic ecotones. However, these changes are highly variable depending on plant species, topographic position, hydrology, soils and other ecosystem properties. Changes in shrub and other vegetation properties are critical to document due to their first-order control on water, energy and carbon balances. This study uses a combination of multi-temporal LiDAR (Light Detection and Ranging) and field surveys to measure temporal changes in shrub vegetation cover over the Wolf Creek Research Basin (WCRB), a 180 km^2 long-term watershed research facility located ~15 km south of Whitehorse, Yukon Territory. This work focuses on the smaller Granger Basin, a 7.6 km^2 subarctic headwater catchment that straddles WCRB's subalpine and alpine tundra ecozones with a wide range of elevation, landscape topography, and vegetation. Airborne LiDAR surveys of WCRB were conducted in August 2007 and 2018, providing an ideal opportunity to explore vegetation changes between survey years. Vegetation surveys were conducted throughout Granger Basin in summer 2019 to evaluate shrub properties for comparisons to the LiDAR. Machine learning classification algorithms were used to predict shrub presence/absence in 2018 based on rasterized LiDAR metrics with up to 97% overall independent accuracy compared to field validation points, with the best-performing model applied to the 2007 LiDAR to create binary shrub cover layers to compare between survey years. Results show a 63.3% total increase in detectable shrub cover > 0.45 m in height throughout Granger Basin between 2007 and 2018, with an average yearly expansion of 5.8%. These changes in detectable shrub cover were compared across terrain derivatives created using the LiDAR to quantify the influence of topography on shrub expansion. The terrain comparison results show that shrubs in the study area are located in and are preferentially expanding into lower and flatter areas near stream networks, at lower slope positions and with a higher potential for topographic wetness. The greatest differences in terrain derivative value distributions across the shrub and non-shrub change categories were found in terms of stream distance, elevation, and relative slope position. This expansion of shrubs into higher-resource areas is consistent with previous studies and is supported by established physical processes. As vegetation responses to warming have far-reaching influences on surface energy exchange, nutrient cycling, and the overall water balance, this increase in detectable shrub cover has a wide range of impacts on the future of northern watersheds. Overall, the findings from this research reinforce the documented increase in pan-Arctic shrub vegetation in recent years, quantify the variation in shrub expansion over terrain derivatives at the landscape scale, and demonstrate the feasibility of using LiDAR to compare changes in shrub properties over time.

ACKNOWLEDGEMENTS

I am extremely grateful to my supervisor Dr. Sean Carey for all of his support and guidance over my time in the Watershed Hydrology Group. From troubleshooting problems with the dGPS in the field house backyard to connecting me with whatever resources I needed to succeed, this work would not have been possible without his continued help and enthusiasm for the science. Special thanks go to Patrick DeLuca for his mentorship and advice throughout my undergraduate and graduate degrees, and for helping me develop the background knowledge and analytical skills to ensure I would be in a position to take advantage of these opportunities.

I would like to acknowledge Dr. Chris Hopkinson & Allyson Fox from the Applied Geomatics Research Group for providing the 2007 LiDAR survey and Dr. Brian Menounos from UNBC for the 2018 survey. Funding for this study was provided by the Global Water Futures and Northern Water Futures program.

Thanks goes to the entire McMaster Watershed Hydrology Group for their support and entertainment in the office over the past 2 years. Special acknowledgement goes to David Barrett, Tyler de Jong, Joseph Desmarais, Fiona Chapman, Erin Nicholls, and Dr. Nadine Shatilla for support in the field; Arsh Grewal and Victor Tang for their help with R and Python scripting; and Dr. M. Graham Clark, Supriya Singh, Keegan Smith, Kelly Biagi, Dr. Luca Fabris, and Ian Martin for their technical advice and willingness to act as a sounding board for my ideas. I would also like to thank Dr. Camile Söthe from the McMaster University Remote Sensing Lab for her advice and expertise in LiDAR processing.

Finally, it would not be possible to name all the amazing people from the McMaster graduate community who deserve recognition for helping distract me from my problems and retain some sanity at the Phoenix every Thursday (and often more).

TABLE OF CONTENTS

LIST OF TABLES

Chapter 2

Chapter 3

LIST OF FIGURES

Chapter 2

Chapter 3

CHAPTER 1: INTRODUCTION

High-latitude ecosystems have experienced substantial warming over the past 40 years, which is expected to continue into the foreseeable future (Hinzman et al., 2005; Overpeck et al., 1997; Tape et al., 2006). Consequently, an increase in vegetation growth has occurred throughout the circumpolar North as documented through remote sensing and plot-level studies (Epstein et al., 2013; Myers-Smith et al., 2011; Sturm et al., 2001a; Tape et al., 2006). Satellite remote sensing has shown a regionally variable but overall increase in normalized difference vegetation index (NDVI), estimated vegetation productivity, and aboveground biomass across the pan-Arctic since 1982, largely based on data from the relatively coarse-resolution NOAA AVHRR sensors (Epstein et al., 2012; Epstein et al., 2013; Tape et al., 2006).

A major component of this change is shrub expansion (shrubbing) in arctic and subarctic ecotones, whereas the migration of boreal forest treeline is less pronounced (Epstein et al., 2013; Tape et al., 2012). Tape et al. (2006) proposed three distinct types of arctic shrub expansion: shrub in-filling, increasing shrub sizes, and expansion into new areas. Most studies to date have focused on individual shrub species in arctic tundra environments, with a notable lack of research on subalpine vegetation development in subarctic environments. Changes in shrub and other vegetation properties are critical to document due to their first-order control on water, energy and carbon balances (Epstein et al., 2013). The presence of tall shrub patches can substantially modify the local environment in taiga-tundra ecotones, decreasing the richness of plant species and altering habitat availability (Wallace & Baltzer, 2019). The cycling of nitrogen, phosphorus, carbon, and methane in tundra ecosystems are all affected by interactions between the abiotic and biotic influences of shrub canopies (Myers-Smith et al., 2011). In addition, both expansion and densification of shrubs decreases surface reflectance and increases absorption of solar radiation, leading to a positive global warming feedback (Ménard et al., 2014).

Changes in the overall water balance, streamflow regimes, and water quality due to vegetation responses to warming have far-reaching implications for northern freshwater ecology (Tetzlaff et al., 2013). Shrub rainfall interception loss is a major component of the water balance in tundra environments, with birch patches reducing effective below-canopy rainfall by up to 30% (Zwieback et al., 2019). The increase in tall shrubs has contributed to a decline in erosion in Arctic streams and floodplain areas, along with an increase in stabilized soil (Tape et al., 2011). The interactions between shrub canopies and snow cover influence soil and permafrost temperatures (Myers-Smith et al., 2011). Increases in shrub cover in Arctic basins lead to increased snow storage, with higher accumulation of snow in shrub tundra largely resulting from exposed shrubs increasing aerodynamic roughness (Essery et al., 2006; Pohl et al., 2007). As a result of complex interactions between net radiation, turbulent transfer, and sensible heat fluxes, snowmelt rates are generally enhanced under shrub canopies compared to sparsely vegetated tundra (Pomeroy et al., 2006). Increased plant biomass also leads to shallower thaw depths due to the insulative effects of vegetation and highly organic soil horizons (Walker et al., 2003). The relative influence of shrubs on local ground shading and active layer thickness versus their effects on large-scale climate warming feedbacks lead to complex potential permafrost responses (Blok et al., 2010; Lawrence & Swenson; 2011). Understanding how vegetation development varies under different conditions is therefore critical for predicting the future of northern watersheds under a rapidly changing climate.

The rates of shrub expansion are not uniform, both throughout the arctic and subarctic ecotones and within individual study areas (Naito & Cairns, 2011a). These changes have been found to be highly variable depending on plant species, topographic position, hydrology, soils and other ecosystem properties (Epstein et al., 2013). Photo pairs from Tape et al. (2006) showed a large percentage of increasing shrubs overall, while these changes were most easily detected on hillslopes and valley bottoms. Naito & Cairns (2011a) found that shrubs preferentially expand into areas with

higher topographic potential for soil moisture. When examining increases in woody vegetation cover in Eastern Nunavik, Quebec, Tremblay et al. (2012) found that these occurred mainly on south-facing slopes, with the rates of expansion varying across slope gradient and altitude. Tape et al. (2006) and Naito & Cairns (2011a) concluded that increases in shrub cover predominantly occurred in or near riparian areas at lower slope positions. Land-surface parameters with influences on vegetation growth such as these are commonly derived from gridded digital elevation models (DEMs) in a GIS environment (Hengl & Reuter, 2009).

1.1 Remote Sensing of Vegetation

1.1.1 Overview

Remotely sensed data can be used along with field surveys to map vegetation over relatively large areas, along with evaluating how land cover and other properties change over time (Langley et al., 2001). As the responses in arctic and subarctic vegetation to warming may occur at fine scales, broad-scale satellite imagery can be ineffective in detecting and quantifying changes (Lantz et al., 2010). Though multi-temporal coarse- to medium-resolution satellite imagery is useful due to its widespread coverage of the pan-Arctic, these sensors cannot capture the heterogeneity of vegetation change within pixels (Naito & Cairns, 2011a; Tape et al., 2012).

In regards to long-term monitoring of arctic vegetation, studies to date have used remotely sensed data from repeated historical airphoto pairs (Naito & Cairns, 2011a; Sturm et al., 2001a; Tape et al., 2012), the NOAA AVHRR (Epstein et al., 2012; Tape et al., 2006), SPOT imagery (Tape et al., 2011; Tape et al., 2012), Landsat imagery (Campbell et al., 2020; Fraser et al., 2011; Tape et al., 2011), and higher-resolution commercial satellites such as the WorldView and QuickBird sensors (Naito & Cairns, 2015). However, conventional sensors such as these have significant limitations for ecological and vegetation-focused applications (Lefsky et al., 2002). Optical imagery is limited by its

inability to sense height or density of vegetation and lack of penetration with cloud cover (Millard & Richardson, 2013). Spectral signatures of woody vegetation such as trees and shrubs are often similar to adjacent lower-stature vegetation such as grasses, leading to potential difficulty in differentiating between classes (Leckie et al., 2005).

1.1.2 LiDAR Remote Sensing of Vegetation

Airborne laser scanning, commonly referred to as LiDAR (Light Detection and Ranging) is an active remote sensing method used to characterize objects at or near the earth's surface where pulses of light are emitted from an aircraft-mounted laser instrument (Farid et al., 2008; Hopkinson et al, 2006; Wehr & Lohr, 1999). When emitted light is reflected back to the sensor above a certain threshold of energy, a single point or "return" is recorded (Roussel et al., 2017). By knowing the speed of light, the location and orientation of the laser emitting and receiving instruments, and the time between pulse emission and its arrival back to the receiver, the location of this return in 3D space can be computed (Hopkinson et al., 2006). LiDAR has become one of the most efficient remote sensing techniques for acquiring detailed and accurate 3D data on landscape topography and vegetation, and can make up for several shortcomings of traditional satellite remote sensing (Wu et al., 2016). As the light pulses from LiDAR sensors can penetrate vegetation cover, they can directly measure the 3D distribution of canopies and the topography below (Lefsky et al, 2002). The addition of vertical information from integrating LiDAR data can reduce the problems in distinguishing vegetation classes with optical imagery alone (Castillo et al. 2012; Ghosh et al. 2014).

Though LiDAR has been shown to reliably estimate forestry metrics such as height, canopy cover, and biomass, obtaining accurate estimates for lower-stature vegetation is more challenging (Estornell et al., 2011; Greaves et al., 2016; Hopkinson et al., 2005; Streuker & Glenn, 2006). The low height of shrub vegetation requires high levels of accuracy in the methodology and

characteristics of the LiDAR data used (Estornell et al., 2011). Hopkinson et al. (2005) found that both low (< 2 m) and high (2-5 m) shrubs display high levels of vegetation surface underestimation compared to field height measurements, with this error representing over 50% of the total shrub height. These errors can be attributed to factors such as the low heights and densities of shrub canopies, sampling errors due to pulse density, and the strong influence of ground surface classification. The relatively open structure and low foliage densities typical of short shrubs can lead to considerable amounts of foliage penetration by the LiDAR pulses before they generate a return, leading to large proportional underestimations in height (Hopkinson et al., 2005). Low sampling rates (i.e. return densities) make LiDAR pulses more likely to miss the highest points of vegetation and underestimate heights compared to field measurements (Zhao et al., 2018), and potentially miss them entirely. As noted in Streuker & Glenn (2006), a LiDAR survey with a return density of $1.2/m^2$ and a footprint diameter of ~20 cm would only sample less than 10% of the actual ground surface. The limitations of laser sensor thresholds for separating first- and intermediate-returns can also be an issue (Greaves et al., 2016).

The accuracy of the DEM and ground-classification routine used to create it has a large proportional influence on LiDAR estimates of low-stature vegetation. In order to measure both topography and vegetation properties above the ground surface, LiDAR returns from ground and non-ground features must be identified and classified. Errors in the creation of a ground surface will propagate to errors in the estimates of vegetation heights above it (Hyyppä et al., 2008). The identification and removal of non-ground points to create bare-earth DEMs in complex environments has proven to be a challenging task (Zhang et al., 2003). Algorithms for ground-classification include slope-based methods using TIN refinement (Axelsson, 1999; Axelsson, 2000; Isenburg, 2019), mathematical morphology-based methods (Zhang et al., 2003), and surface-based methods (Zhang et al., 2016). For a more exhaustive list of existing ground-classification algorithms, see Montealegre et

al. (2015). When considering these inherent difficulties associated with low vegetation, accurate LiDAR surveys and ground-classification routines are needed for reliable and reproducible results (Estornell et al., 2011).

Due to the challenges in estimating shrub heights from lower-resolution LiDAR (Estornell et al., 2011; Greaves et al., 2016; Hopkinson et al., 2005; Streuker & Glenn, 2006), the capability to model shrub presence and absence has been explored. This has been accomplished through simple presence/absence thresholds based on LiDAR-derived canopy height models (Estornell et al., 2011) and surface roughness values based on the standard deviation of LiDAR return heights (Streuker & Glenn, 2006). More recently, supervised machine learning algorithms have been used along with airborne LiDAR and optical imagery to successfully classify landscapes such as wetlands (Millard & Richardson, 20103; Millard & Richardson, 2015), tropical forests (Sothe et al., 2019), urban environments (Carlberg et al., 2009) and water areas (Smeeckaert et al., 2013), among others. However, there is limited research on the use of these methods to detect and/or classify low-stature vegetation.

One machine learning classifier that has been commonly used in landscape classifications (Belgiu, 2016) is the random forests (RF) algorithm proposed by Breiman (2001). This is an ensemble learning method that is based on successive Classification and Regression (CART)-like trees using different bootstrapped samples of training data, has few user-defined parameters, and is robust against overfitting (Liaw & Weiner, 2002; Millard & Richardson, 2015). The support vector machines (SVM) group of machine learning classifiers is another widely used algorithm that functions on the basis of linearly separable classes (Richards, 2013). The SVM employs optimization algorithms to locate optimal boundaries between classes, using a separating hyperplane based on the selected kernel function (Huang et al., 2002). Duro et al. (2012) compared the accuracy of classifying

agricultural landscapes using RF and. SVM, finding no statistically significant differences in the results.

1.1.3 Change Detection with Multi-Temporal LiDAR

Forestry metrics such as stand height, wood volume, and above-ground biomass are commonly estimated from LiDAR point clouds using statistical models (Roussel et al., 2017). LiDAR has been used to evaluate changes in properties such as these between surveys, which can be logistically difficult as the structure of point clouds is dependent on the LiDAR instrument used, sensor configurations, and flight details (Bater et al., 2011; Roussel et al., 2017). Although there is a lack of research on using multi-temporal LiDAR to evaluate changes in low stature vegetation properties, Streuker & Glenn (2006) and Estornell et al. (2011) suggested that their threshold-based presence/absence methods could feasibly be used to compare changes in shrub cover between surveys.

The stability of forestry metrics derived from different LiDAR point clouds has been explored previously, with comparisons between surveys with identical sensors and parameters (Hopkinson et al., 2008; Naesset, 2004), the effects of sensor configurations and flight parameters, (Naesset, 2009; Roussel et al., 2017), and between different sensor instruments used (Bollandsås et al., 2013; Cao et al., 2016; Hopkinson et al., 2008; Naesset, 2009; Zhao et al., 2018). Hopkinson et al. (2008) concluded high-resolution LiDAR datasets acquired from comparable surveys can detect growth in homogenous red pine conifer plantations at an annual timestep, but increased stand heterogeneity such as in natural environments and different survey configurations would introduce more uncertainty.

The effects that acquisition parameters have on the structure of point clouds should be considered when evaluating metrics over separate surveys (Roussel et al., 2017). When sampling

rates are lower (resulting in a lower return density), LiDAR pulses are more likely to miss the highest points of the vegetation and underestimate heights compared to field measures (Zhao et al., 2018). However, due how variations in pulse density are accompanied by variations in aircraft altitude and therefore return footprint size, conclusions such as these may be overly simplistic (Roussel et al., 2017). Such biases caused by different sensor configurations must be corrected for in order for comparisons between them to be valid. Cao et al. (2016) found that even with the differences between an older ALTM-3100 discrete-return and newer Riegl LMS-Q680i full waveform unit, forestry height metrics could be efficiently compared over 6 years between surveys after coregistration of the point clouds.

1.2 Research Objectives

The primary objective of this study is to use a combination of airborne LiDAR and field methods to measure spatial changes in vegetation over 11 years within a well-studied subarctic mountain basin. The potential for LiDAR data to accurately capture changes in shrub height between survey years is explored along with quantifying changes in detectable cover using supervised machine-learning classifications of shrub presence and absence. Due to the documented heterogeneity of shrub expansion within individual study areas, terrain derivatives are used for quantitative comparisons of these changes over different landscape positions. The wide range of elevation, landscape topography, and vegetation within the study area will make these results applicable to other northern environments. Considering the rapid change to circumpolar systems, results from this study help: 1) quantify how shrub vegetation cover has changed over time in an alpine subarctic ecosystem, and 2) link these changes to ecotone and physiographic variables such as elevation, aspect, slope position, topographic wetness, and proximity to riparian areas.

CHAPTER 2: METHODS

2.1 Study Area

This study was conducted in Granger Basin, a ~7.6 km^2 subarctic headwater catchment located in the west-central region of the Wolf Creek Research Basin (WCRB) (Carey et al., 2013). The WCRB is a ~180 km^2 long-term watershed research facility located ~15km south of Whitehorse, Yukon Territory with over 20 years of comprehensive meteorological data on record (Janowicz, 1999; Rasouli et al., 2019).

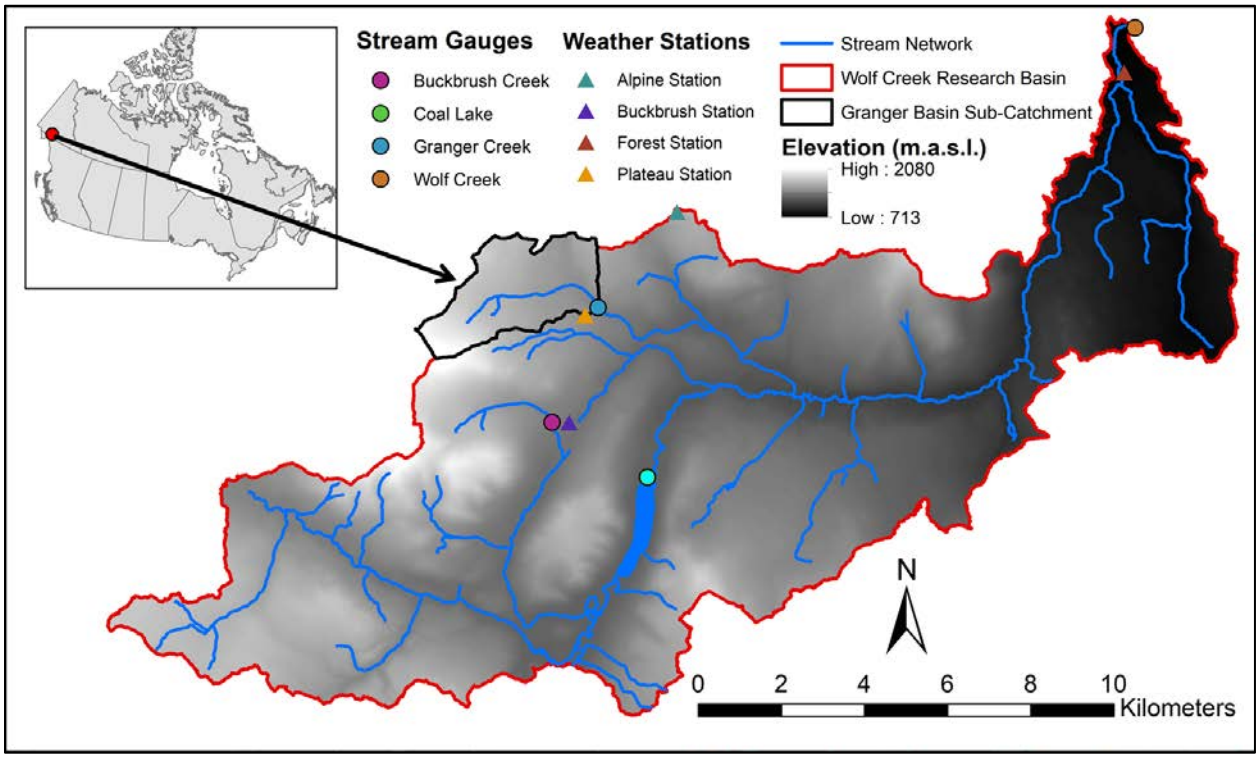

Figure 2.1: Study area of the Granger Basin sub-catchment, located within the larger WCRB

Granger Basin straddles the subalpine and alpine tundra ecozones of the WCRB, with an elevation range of 1356 to 2080 m.a.s.l. (as referenced to the CGVD28 geoid). The climate is characterized as continental subarctic, with mean annual precipitation of ~400 mm of and a mean annual temperature of -3 ^{o}C (Carey et al., 2013). The lower basin contains a mix of low-lying grasses, willow shrubs, and dwarf birch shrubs, with taller shrubs (>2 m) along the riparian corridor and few isolated patches of white spruce (Piovano et al., 2019). At upper elevations, land cover is

dominated by bare rock, short tundra mosses, and grasses (Rasouli et al., 2019). A more comprehensive description of Granger Basin is found in McCartney et al. (2006).

2.2 LiDAR Acquisition

Airborne LiDAR surveys of the WCRB were conducted in August 2007 by Dr. Chris Hopkinson and the Applied Geomatics Research Group (AGRG) and August 2018 by Dr. Brian Menounos (University of Northern British Columbia). The 2007 survey was delivered from AGRG as 115 separate tiles in the ASPRS .las file format, each measuring 2 km by 2 km with 20 m buffers. The data was originally projected into the XY coordinate system NAD 1983 UTM Zone 8N, with elevations referenced to the CGVD28 geoid (Véronneau et al., 2001). However, no projection information was assigned to the actual LAS files as provided. More in-depth details of the LiDAR preprocessing from survey to delivery can be found in the survey report (AGRG, 2008) and Hopkinson & Chasmer (2009). According to testing from the sensor manufacturer (Ussyshkin et al., 2006), the ALTM 3100 discrete-return unit has a reported accuracy of 15 cm (as one standard deviation) at a flying height of 1200 m.a.g.l. The sensor's minimum pulse separation required to obtain multiple returns is 2.14 m (Ussyshkin & Theriault, 2011). The 2018 survey was delivered as a single compressed .laz file, which was extracted to the more commonly used .las format using LASzip (Isenburg, 2012). The data was originally projected into the WGS 1984 UTM Zone 8N XY coordinate system, with elevations referenced to the WGS84 ellipsoid. According to testing from the sensor manufacturer, the Riegl Q-780 full-waveform unit used in the survey has a reported accuracy of 2 cm at a range of 250 m.

Table 2.1: Flight parameters and scanner properties of both LiDAR surveys used

Survey Date	**Sensor Used**	**Flying Height (m.a.g.l.)**	**Pulse Frequency (Hz)**	**Scan Angle (degrees)**	**Approx. Return Density (m^{-2})**
Aug. 11, 2007	Optech ALTM 3100	1350 - 1550	3300	+/-23	0.67
Aug. 18, 2018	Riegl Q-780	3000 - 3030	400	+/-33	11.9

2.3 Field Data Collection

2.3.1 LiDAR Validation

A Hemisphere S320 GNSS RTK system was used to collect 371 differentially-corrected GPS (dGPS) points on relatively hard, flat surfaces such as roads and established trails throughout the extent covered by both LiDAR surveys. Only averaged base station positions and points that were able to capture an RTK Fixed solution were included in the validation set used to evaluate LiDAR survey accuracy. These points were collected in the NAD 1983 UTM Zone 8N XY coordinate system, with heights referenced to the WGS84 ellipsoid. 164 total dGPS points from the vegetation surveys and shrubline mapping were also captured with an RTK Fixed solution (including averaged base station estimates). The base station receiver was configured to store raw logging data every second, which can be used for post-corrections of stored coordinates for greater positioning accuracy.

2.3.2 Shrubline Mapping

When examining preliminary HAG (height above ground) models from both LiDAR datasets, there were a significant amount of returns >50 cm above the ground surface which were unlikely to be vegetation due to their high elevations within the alpine tundra ecozone (>1650 m.a.s.l.). In order to help examine the differences between true shrub cover and these artifacts, Granger Basin's shrubline was delineated using the same dGPS unit as used for the LiDAR validation. Starting at the south-west corner of the basin and moving north-east, coordinates of the

highest shrub patches were recorded with the dGPS, then the shrubs were photographed and their heights were measured with an avalanche probe where the dGPS point was taken. As the majority of these points were captured with an RTK Fixed solution, they were included in the validation set for vegetation. With the highest shrubs in Granger Basin recorded, any non-ground LAS returns above this line could be safely assumed to be either large rocks/boulders, flightline noise, or some other LiDAR survey error.

2.3.3 Vegetation Surveys

29 vegetation transects were spread across Granger Basin in order to evaluate vegetation and landscape properties for comparison to LiDAR metrics. Each transect was located on slopes with a roughly consistent slope aspect and obvious shrub presence as interpreted from preliminary LiDAR HAG models and pan-sharpened WorldView-2 imagery. Transects were spread throughout the basin in order to get a roughly even distribution between elevation and aspect directions and capture maximum variability. These pre-identified target sites were navigated to using the Collector for ArcGIS mobile application, where a decision was made on whether they were acceptable locations for a transect before surveying.

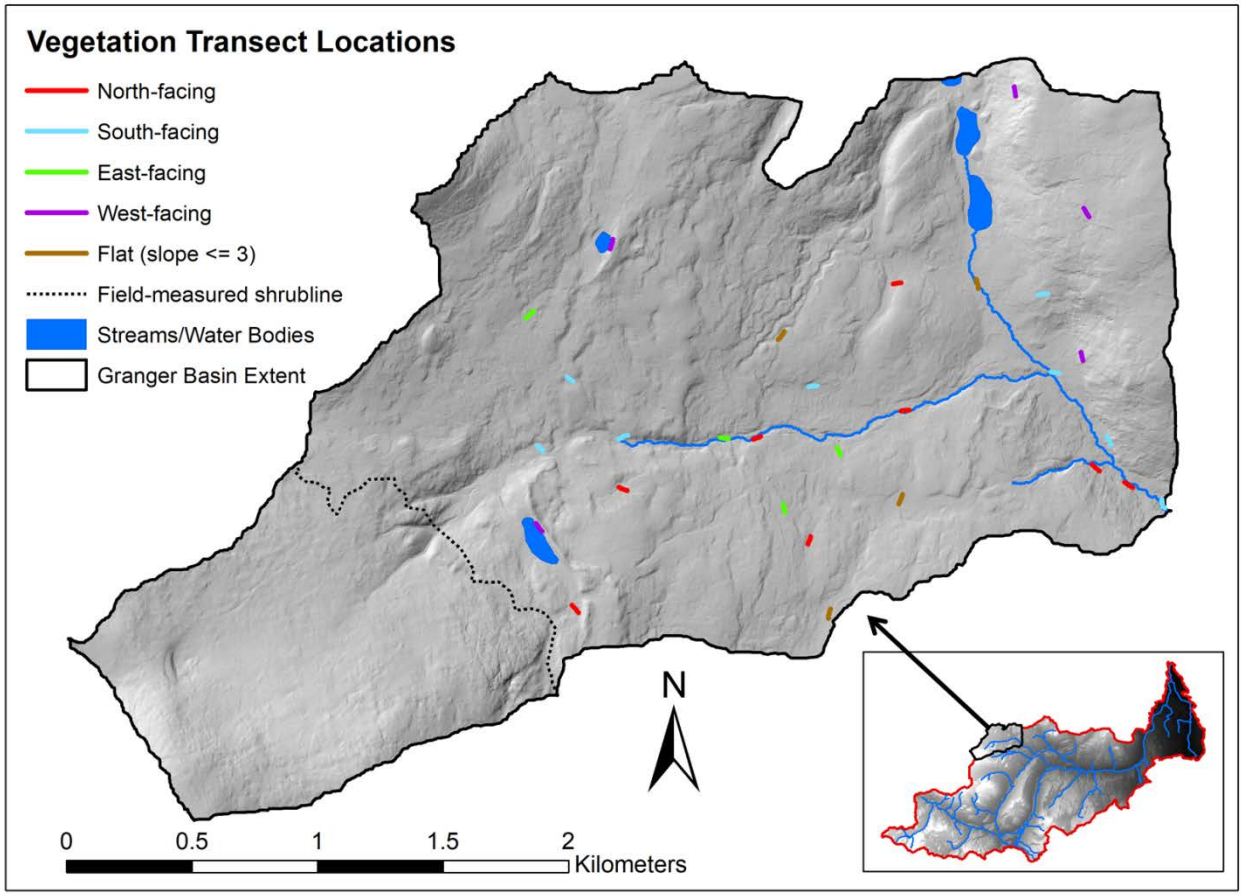

Figure 2.2: Location of vegetation transects within Granger Basin along with the field-measured shrubline

The plot and transect structure were roughly modeled after the shrub transects from Tape et al. (2012). Each 40 m transect consisted of 5 circular plots with a 1 m radius, spaced out at every 10 m using a pre-measured rope. Each plot used a bamboo post to mark out the center, with a rope attached with markings at 50 cm and 1 m. These plot centroids were then mapped using the dGPS and photographed. At each plot, several characteristics were recorded and/or measured along with any relevant notes (weather conditions, cloud cover, LAI 2200 lens cap used, etc.).

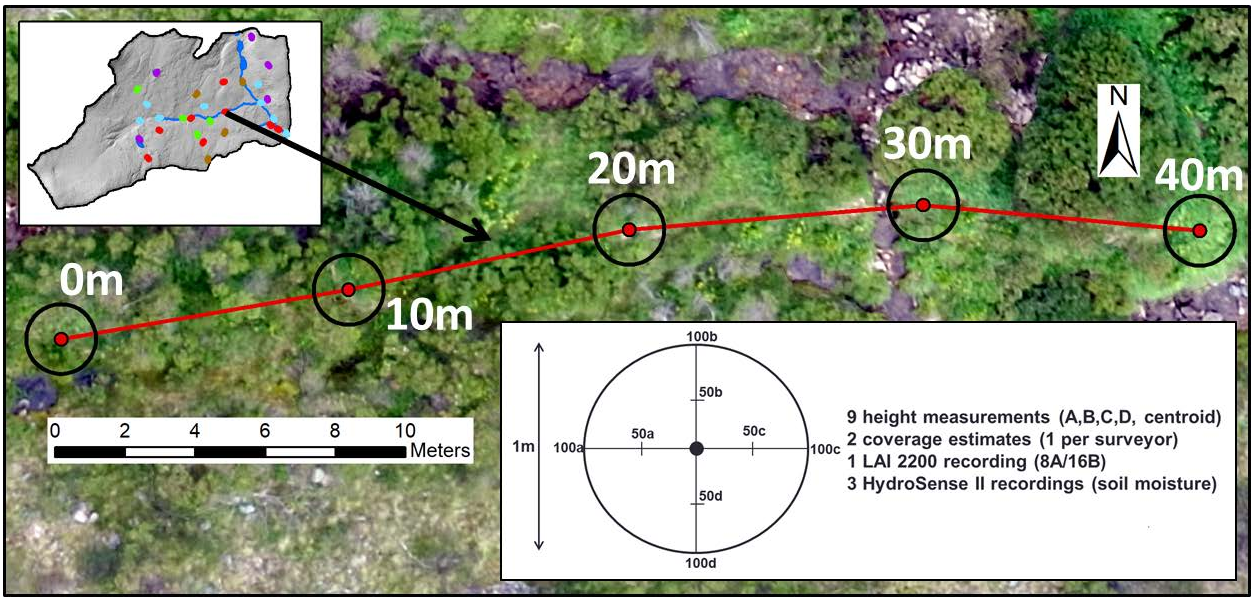

Figure 2.3: Example vegetation transect in Granger Basin along with diagram of survey methodology

Vegetation height was measured using an avalanche probe at 9 regularly-spaced points throughout each plot (A, B, C, D, plot center), with the highest species at each point recorded. The percent coverage of each species or land cover classification present within the plot was estimated by each surveyor present and averaged to get a final value. Volumetric water content at 20 cm depth was measured using a HydroSense II soil moisture probe at 3 representative locations per plot. Leaf area index (LAI) was also recorded throughout the plot with a single-wand LAI 2200 using 8 above-canopy measurements and 16 below-canopy measurements.

Table 2.2: Variables measured in vegetation surveys and equipment used

Variable measured	**Repetitions (per plot)**	**Instrument used**
Vegetation height	9	Avalanche probe
Percent cover (per species)	2	n/a (visual estimate)
Volumetric water content	3	HydroSense II
Leaf Area Index	8A/16B	LAI 2200
GPS coordinates	1	Hemisphere S320 GNSS RTK

2.4 Field Data Processing

2.4.1 LiDAR Validation

dGPS points taken during the field campaign were used to determine the accuracy of both LiDAR surveys. After conversion of the raw base station .BIN files to RINEX format, post-processing of the dGPS points was done using Natural Resources Canada's Precise Point Positioning (CSRS-PPP) and TRX tools. CSRS-PPP uses precise GPS orbit and clock products generated through international collaboration to improve positioning results by a factor of 2 to 100 when compared to uncorrected positions (Tétreault et al, 2005). As CSRS-PPP computes estimated heights using the GRS80 ellipsoid, the estimated coordinates from PPP were referenced to the WGS84 ellipsoid (identical to ITRF 2008 reference frame) using the TRX tool so that they would match the 2018 LiDAR's vertical and horizontal spatial references. Positional shifts calculated using CSRS-PPP and TRX were applied to the original FieldGenius output coordinates in R Statistics (R Core Team, 2019), which were then exported as CSVs and shapefiles for further use.

2.4.2 Vegetation Transects

The dGPS points representing each transect were extracted from each MicroSurvey FieldGenius project file containing their respective coordinates and saved in CSV format. Each transect CSV was given new fields to store the original transect ID and the plot increment that each point represented. Shrub species were separated into willow, dwarf birch, and dead shrub categories based on dominant plot area according to the averaged percent cover estimates. Dead shrubs were categorized as a separate class, as they were difficult to differentiate into birch or willow but their aboveground biomass would still generate LiDAR returns.

After the vegetation metrics were calculated for each transect and plot, they were appended as new fields to transect CSVs converted from the original FieldGenius project files. Plot coordinates

were post-processed using CSRS-PPP in the same manner as the validation set. Once the field measures were attached to their respective plots, each transect CSV was converted to shapefile format based on their final averaged Northing and Easting fields and buffered to radii of 50 cm and 100 cm in ArcPy. This preparation gave 29 new shapefiles representing all transects for use in extracting the LAS metrics within their respective plots. Each transect shapefile contained 5 individual circular polygons with 100 cm radii, one for each plot increment (0, 10, 20, 30, 40 m). This gave 145 total plots with field measures to compare with extracted LiDAR metrics..

2.5 LiDAR Pre-Processing

2.5.1 Data Preparation

As the 2007 and 2018 datasets were surveyed using different spatial references based on different datums, these had to be standardized so that both surveys represented the same locations in XY space. The 2007 point cloud was also provided without projection information explicitly assigned to the LAS files, which were assigned their original projection of NAD 1983 UTM Zone 8N to the 2007 tiles using las2las (Isenburg, 2019). A datum transformation was then applied to the 2018 point cloud in ArcGIS Pro (ESRI, 2019) to transform the tiles from their original projection in WGS 1984 UTM Zone 8N and match the 2007 survey's spatial reference. The vertical coordinate systems were also different between the two datasets, as heights from the 2007 survey were based on the CGVD28 geoid while 2018 heights used the WGS 1984 ellipsoid. Respective vertical coordinate systems were assigned to the point clouds using the PDAL library (PDAL Contributors, 2019), then elevations from the 2018 point cloud were transformed to the CGVD28 geoid model using LAStools and GDAL (GDAL/OGR contributors, 2019).

The original 117 GB point cloud for the 2018 survey was subdivided into individual tiles using lastile (Isenburg, 2019), each measuring 500 m by 500 m with 30 m buffers on either side to avoid edge effects when processing. Pre-existing buffers within the 2007 point cloud provided by

AGRG were not explicitly flagged during their creation in TerraScan, and therefore had to be identified and removed through ArcPy and R scripting to avoid duplication artifacts in buffer zones. These new LAS files were then merged and re-tiled to the same specifications as the 2018 data.

Though the 2007 survey return density has been reported as ~1/m^2 (AGRG, 2008; Chasmer et al., 2008; Hopkinson & Chasmer, 2009), after clipping out duplicate points in buffer zones it was found to only contain ~0.67 returns/m^2 through testing in both LAStools and lidR. As lower sampling rates make LiDAR pulses more likely to miss the highest points of vegetation and underestimate heights compared to field measures (Zhao et al., 2018), the differences in return density between the 2018 (~11.9 returns/m^2) and 2007 surveys (~0.67 return/m^2) had to be accounted for. The 2018 survey was thinned to give the area covering Granger Basin an average density of 0.67 returns/m^2 to match with 2007 by retaining only a specified fraction of the original points using las2las (Isenburg, 2019).

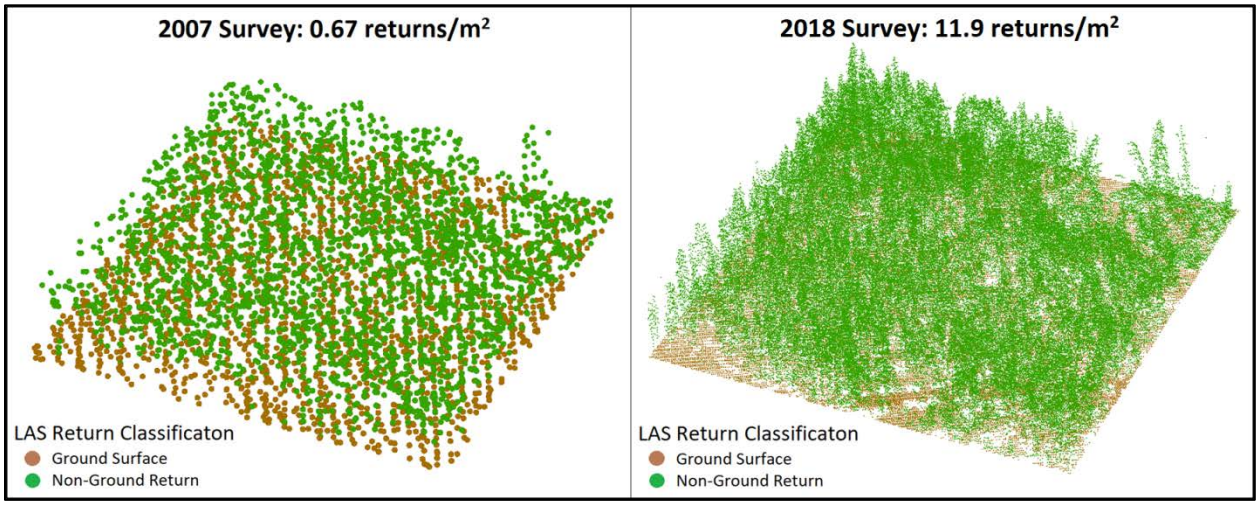

Figure 2.4: Height-normalized 100 x 100 m tile of WCRB forest monitoring station showing resolution differences between surveys

2.5.2. Ground Classification

Due to the inherent difficulties associated with LiDAR measurements of low-stature vegetation, accurate ground-classification routines are essential for valid results (Estornell et al., 2011; Hopkinson et al., 2005). If enough non-ground returns (i.e. those generated from vegetation) are included within the LiDAR-derived ground surface, canopy heights over this surface will be underestimated compared to field measures. Conversely, if topography such as ridges is not included in the ground surface, these will artificially overestimate any height-above-ground metrics.

The dGPS points from the vegetation surveys and shrubline mapping captured with a Fixed RTK solution were used in order to compare the accuracy of different ground-classification algorithms and parameter selections on steeper and more thickly-vegetated surfaces than the validation points. Within the LAStools software suite (Isenburg, 2019), the lasground and lasground_new functions use a variation of the Axelsson (2000) algorithm. This method uses an iterative filtering method based on progressive Triangular Irregular Networks (TIN) densification constructed using the point cloud. Other ground-classification algorithms available through the lidR package's lasground function are the Cloth Simulation Filter (csf) and Progressive Morphological Filter (pmf) functions (Roussel & Auty, 2019). The csf function is a strict implementation of the Zhang et al. (2016) algorithm, which inverts the point cloud and fits a rigid cloth to the inverted surface. The pmf function is a modified implementation of the Zhang et al. (2003) algorithm, which applies a progressive morphological filter with different thresholds at different scales to the point cloud to detect non-ground returns.

Each of these different algorithms was used to ground-classify the 2007 and thinned 2018 point clouds with several different combinations of parameter settings. Ground returns from each new point cloud were directly compared to dGPS point elevations using lascontrol, while elevations from rasterized bare-earth DEMs generated from these returns were also compared to the dGPS points in ArcGIS Desktop. Shaded relief maps were created for each new bare-earth DEM to visually

inspect if low-stature vegetation was mistakenly included as part of the ground surface. The version of the Axelsson (2000) adaptive TIN algorithm in LAStools was found to perform best in terms of removing vegetation from the bare-ground surface while still preserving topographic detail. These ground-classified returns were interpolated to bare-earth DEMs using the lidR package's *knnidw* function (Roussel & Auty, 2019), as this gave a smoother and more natural grid surface than las2dem's TIN-based interpolation algorithm at low return densities. LAS files were gridded to bare-earth DEMs of various resolutions depending on their intended purpose using a 2nd power Inverse Distance Weighting function based on each cell center node's 10 nearest neighbours.

2.5.3 LiDAR Validation

After post-corrections were applied to field-collected dGPS points within the LiDAR validation sets (see section 2.4.1), these modified coordinates were compared directly to returns from the point clouds as well as LiDAR-derived raster DEMs to evaluate the accuracies of both surveys. lascontrol is a tool that computes the height of a LiDAR point cloud at specified x and y control point locations by triangulating nearby points into a TIN, then reports the height difference relative to these control points (Isenburg, 2019). This was used to compare elevations from corrected dGPS validation points to LiDAR returns and directly evaluate survey accuracy using CSV outputs from lascontrol in R. Last- and ground-classified returns were compared to dGPS elevations for the 2007, original 2018, and thinned 2018 point clouds by subtracting the dGPs elevations from the LiDAR z-values.

All DEMs used for validation were interpolated at a 1m resolution using lidR's *grid_terrain* and *knnidw* functions with identical parameters. As the *grid_terrain* function only considers ground-classified returns, last-returns were extracted from the point clouds using las2las and coerced to Class 2 (ground) using ArcGIS Pro so that they could all be included in the DEM creation. After rasterizing each respective set of LAS tiles, DEM elevations at control point locations were extracted using

ArcGIS Desktop 10.7 in order to compute height differences. Shapefile attribute tables containing the respective elevations were then imported into R for analysis.

2.5.4 Height Normalization

After ground classification, the height above ground (HAG) of the resulting point cloud was computed using lasheight (Isenburg, 2019). This tool triangulates ground-classified returns into a temporary TIN and replaces the z-values of non-ground points with their computed height above the ground surface. Preliminary HAG derivatives from both LiDAR surveys showed clear non-shrub artifacts along overlapping flightlines, which were confirmed to be areas of poor vertical accuracy through lasoverlap (Isenburg, 2019). As these artifacts were greater than some measured vegetation heights, they led to inaccurate HAG-derived shrub metrics (Streuker & Glenn, 2006). This issue was substantially improved by extracting individual flightlines and processing them separately, then merging the files back together and re-tiling after the height normalization was complete. Metrics from these corrected point clouds were then used as estimates of field-measured vegetation heights.

2.6 LiDAR Derivatives

2.6.1 Vegetation Height Comparisons

LAS metrics from the height-normalized point clouds were extracted for each buffered plot radius using lascanopy (Isenburg, 2019) and appended to new shapefiles to compare to the average and maximum vegetation heights measured in the field. Metrics were extracted from the 2007 point cloud, original 2018 point cloud, and the 2018 point cloud after thinning it to match the 2007 survey return density. These values were compared to field measures for each plot to evaluate how well the LiDAR could estimate the average and maximum heights within the 1 m plots.

2.6.2 Shrub Cover Estimation

Along with the shrub height estimates, the ability of the 2018 LiDAR survey to model shrub presence and absence was explored by comparing results from the thinned point cloud to field surveys. As most of the vegetation plots had a varying degree of shrub cover within them, detectable shrub presence for model training and validation also had to be defined using a cutoff based on minimum height and/or cover values. Previous work has also found that operational lower limits for vegetation height determination may exist (Streuker & Glenn, 2006). Plots where the average field-measured height was greater than 45 cm (~RMSE of 2007 LiDAR last-return surface in vegetated areas) were therefore considered to be shrub points, giving an N of 114 for presence. An additional 114 absence points were created by generating random points within Granger Basin and interpreting which did not have shrub cover through LiDAR derivatives and pan-sharpened Worldview-2 imagery. After setting a random seed to ensure reproducibility, these points were separated into a 70% training set (160 observations) to train the predictive models and a 30% validation set (68 observations) to independently assess the classification accuracies.

Binary supervised classifications of shrub presence/absence were conducted using rasterized LiDAR metrics from the thinned 2018 point cloud through machine learning algorithms in R. Model inputs were gridded from LAS format into raster layers with 2 m spatial resolution, with values taken from a 3x3 pixel moving window using lascanopy (Isenburg, 2019). For the vegetation density metrics, the 0.45 m threshold was chosen due to the 2007 LiDAR last-return RMSE over variable terrain with vegetation cover. This threshold removed the majority of low noise in clearly non-shrubbed areas for derivatives from both point clouds. Topographic indices other than elevation were not included as predictors since the end goal of this study was to compare shrub expansion across them. Intensity metrics were standardized between surveys as the ALTM-3100 used in the 2007 study produced a different range of intensity values than the Riegl Q-780 used in 2018. The

rasterized LiDAR metrics that were considered for use as predictor variables are presented in Table 2.3.

Table 2.3: Original list of rasterized LiDAR metrics used as predictors for shrub classifications, before removal of highly-correlated variables

Variable	**Description**	**Generating Software**
Avg. HAG	Average HAG of LiDAR	LAStools (lascanopy)
Max. HAG	Maximum HAG of LiDAR	LAStools (lascanopy)
Std. of HAG	Standard deviation of HAG values of LiDAR	LAStools (lascanopy)
Count >45cm	Total number of returns above cover cutoff (45cm HAG)	LAStools (lascanopy)
Cover >45cm	Number of first returns above cover cutoff divided by number of all first returns	LAStools (lascanopy)
Density >45cm	Number of all returns above cover cutoff divided by number of all returns	LAStools (lascanopy)
Max INT	Maximum intensity of LiDAR	LAStools (lascanopy)
Avg. INT	Average intensity of LiDAR	LAStools (lascanopy)
DEM	Elevation of interpolated ground return surface	lidR (grid_terrain, knnidw)

To obtain reliable classification results when using affordable numbers of training pixels, predictors that do not aid discrimination between classes should be removed (Richards, 2013). As several of these original input variables were expected to be highly correlated due to their derivation from identical physical processes (6 HAG-based, 2 INT-based), Spearman's rank-order correlation coefficient was used to reduce dimensionality and ensure that only less-correlated variables were included in the landscape classifications. After the most highly-correlated variables were identified, a qualitative decision was made on which to retain for use in the final classifications.

The reduced set of predictor variables was used to classify Granger Basin into shrub and non-shrub classes using the random forests (RF) and radial-kernel support vector machine (SVM) machine learning classifiers in R (Liaw & Weiner, 2002; Meyer et al., 2019). Optimal

hyperparameter settings for these algorithms were determined using a grid search with 5 repeats of 10-fold cross-validation based on a training set of observations. The overall independent accuracy of the shrub cover classifications was assessed using the 30% validation set according to an error matrix as in Congalton & Green (2008). The effect of training and validation set selection on classification accuracy was explored by running 25 separate classifications for each method using different random seeds and computing the overall error and kappa coefficients for each exported error matrix (Leutner et al., 2019). The total area classified as shrub and non-shrub were also computed and recorded for each classification. Class stability over each of the iterations was assessed to see which areas of Granger Basin were most frequently classified as shrubs using similar methodology as Millard & Richardson (2015).

The classification model with the best overall independent accuracy and class stability using the thinned 2018 point cloud was applied to the 2007 LiDAR survey to create raster layers representing shrub cover in Granger Basin for both 2007 and 2018. These were reclassified so that shrub pixels were given a value of 1, with non-shrub pixels having a value of 0. The 2007 raster was then subtracted from 2018 so that the resulting vegetation change layer had three categories: 1 = gain, 0 = no change, and -1 = loss (Naito & Cairns, 2011a). Layers representing stable shrub and stable non-shrub pixels were also created from pixels with identical values of 1 and 0 respectively in both classifications.

Due to the presence of large rock fields in the upper Granger Basin that resemble vegetation in terms of LiDAR HAG metrics, a small percentage of the shrub-classified pixels in both years (0.14% in 2007, 0.53% in 2018) were erroneously located above the true field-measured shrubline (see section 2.3.1). These areas were therefore masked out of the final shrub layers. All pixels located within known water bodies were also removed, as lake extents differed slightly between the 2007 and 2018 survey leading to artifacts in the change layer. After these corrections, pixels from the 4 shrub change classes (gain, loss, stable shrub, and stable non-shrub) were used for the terrain comparisons.

2.6.3 Terrain Comparisons

As the rates of shrub expansion vary across individual study areas (Naito & Cairns, 2011a; Tape et al., 2006; Tremblay et al., 2012,), several terrain derivatives were created in SAGA GIS (Conrad et al., 2015) from a 2 m resolution bare-earth DEM created using the 2018 point cloud so that changes in shrub cover could be quantified and compared across different landscape properties. Elevation, slope gradient, and relative slope position were used to compare how the shrub changes vary over their influences on environmental phenomena (Tremblay et al., 2012; Walker, 2000). Slope aspect was included in the comparisons due to its significance in regards to solar insolation, evapotranspiration, and flora distribution/abundance (Wilson & Gallant, 2000). The sine and cosine functions were used to convert the original aspect values of 0-360 into continuous gradients of northness and eastness, respectively (Cardoso, 2020; Guisan et al., 1999). Another aspect layer with the original values of 0-360 was retained for categorical comparisons based on cardinal direction, but with any cells with a slope less than 3 degrees reclassified as flat (-1) as the influence of aspect at this level would be minimal (Nichols et al., 2008).

The influence of proximity to stream networks on shrub expansion was also explored, as Tape et al. (2006) and Naito & Cairns (2011a) found that increases in shrub cover predominantly occurred in or near riparian areas. A grid of all interconnected stream and lake cells in Granger Basin was created using a flow direction grid derived using ArcGIS Hydrology toolset (D8 algorithm), pan-sharpened WorldView-2 imagery, LiDAR intensity metrics, and knowledge from site visits. This stream network was imported along with the bare-earth DEM into SAGA GIS where raster layers representing Euclidean distance, horizontal overland flow distance, and vertical distance to the channel network were computed. The topographic wetness index (TWI) as proposed by Beven and Kirkby (1979) provides a means for assessing and characterizing topographic conditions that control soil moisture and groundwater flow (Sørenson et al., 2006). It is calculated based on a pixel's

upslope contributing area and slope percent), with higher values having more potential for wetness than surrounding areas. A modified version of the TWI algorithm called the SAGA Wetness Index (SWI) was used for this study as it gives more realistic, higher potential soil moisture values in topographic incisions when compared to the original index (Bohner et al., 2006).

Relationships between the terrain derivatives used were explored through Spearman's rank-order correlation coefficient. Terrain raster values that fell within each of the change classes (gain, loss, stable shrub, and stable non-shrub) as well as the overall Granger Basin were extracted as vectors in R for statistical analysis. For the continuous variables, one-sided pairwise Wilcoxon rank-sum tests were used to determine whether the frequency distributions of pixels in increasing or stable shrub classes were statistically different from areas of shrub loss, stable non-shrub, or Granger Basin overall. The terrain derivatives used to evaluate shrub expansion and the alternative hypothesis used for the Wilcoxon rank-sum tests are shown in Table 2.4:

Table 2.4: Terrain derivatives and hypothesis used for testing with Wilcoxon rank-sum tests among shrub change classes

Terrain Derivative	**Hypothesis Tested**
Elevation (m.a.s.l.)	Lower elevations are preferential
Slope gradient (^{o})	Flatter areas are preferential
Northness (dimensionless)	South-facing slopes are preferential
Eastness (dimensionless)	East-facing slopes are preferential
Euclidean distance to stream network (m)	Proximity to streams is preferential
Overland flow distance to stream network (m)	Proximity to streams is preferential
Vertical distance to stream network (m)	Proximity to streams is preferential
SAGA wetness index (dimensionless)	Higher topographic wetness is preferential
Relative slope position (dimensionless)	Lower slope positions are preferential

To illustrate shrub change variation across ranges of landscape properties, values from each terrain derivative raster were binned into 5 classes based on the Jenks Natural Breaks classifier in ArcGIS Desktop (Tremblay et al., 2012) which seeks to group similar values and maximize differences between classes (de Smith et al, 2018). The percentage of total pixels in each shrub change category falling into individual terrain value classes was tabulated along with the LiDAR survey extents within Granger Basin as a whole.

CHAPTER 3: RESULTS & DISCUSSION

3.1 LiDAR Validation

When comparing ground-return and last-return elevations to dGPS points from the validation sets (Table 3.1), the 2007 LiDAR survey accuracy (14 cm and 9 cm respectively) was within the positional accuracy listed in the ALTM 3100 sensor documentation of 15 cm at 1-sigma (i.e. one standard deviation) at similar flight elevations (Ussyshkin et al., 2006). The 2 cm accuracy reported in the Riegl Q-780 technical documentation is for a distance of 250 m, which is difficult to compare to the actual flight elevation of 3000-3030 m.a.g.l. However, the 2018 survey accuracy of 6 cm at 1-sigma for both last- and ground-returns was a high enough level of confidence for the purpose of this study. Accuracies from the 2018 point cloud (Table 3.1) were similar before and after thinning to match the 2007 return density. Positional errors were much higher on the complex vegetated terrain within Granger as compared to the flat surfaces in the validation set, as expected. The increased RMSE of 44 cm for last-returns in the 2007 dataset was used as a benchmark for removing low noise in the shrub cover classification predictor variables (see section 2.6.2).

Table 3.1: LiDAR return height errors vs. dGPS position (m) over different land cover types from original 2018, thinned 2018, and 2007 point clouds. AvgAbs represents the average absolute difference between dGPS and LiDAR return elevations.

	2007		**2018 (Original)**		**2018 (Thinned)**	
	Roads	Vegetation	Roads	Vegetation	Roads	Vegetation
Last-returns						
Avg	-0.09	0.16	0.06	0.30	0.06	0.23
AvgAbs	0.10	0.28	0.07	0.31	0.07	0.26
Min	-0.60	-0.64	-0.08	-0.20	-0.08	-0.47
Max	0.38	1.9	0.20	1.76	0.21	1.56
SD	0.09	0.41	0.06	0.29	0.06	0.30
RMSE	0.13	0.44	0.08	0.41	0.08	0.37
Ground returns						
Avg	-0.17	-0.17	0	-0.08	-0.01	0.15
AvgAbs	0.18	0.21	0.05	0.13	0.05	0.20
Min	-0.79	-0.92	-0.48	-1.19	-0.48	-0.47
Max	0.12	0.37	0.15	0.30	0.15	1.28
SD	0.14	0.21	0.06	0.18	0.06	0.23
RMSE	0.22	0.27	0.06	0.20	0.06	0.28

3.2 LiDAR Vegetation Height Comparisons

3.2.1 Overall Accuracy

Due to the low return density of the 2007 LiDAR and resulting thinned 2018 point cloud, 6 plots did not contain a LAS return for 2007 while 1 plot was missing for the 2018 survey. This reduced the sample size for viable comparisons between years from 145 to 139 plots (as a single plot did not contain a 2007 or thinned 2018 return), while the sample size for comparing the accuracies of the original and thinned 2018 point clouds was reduced to 144. 64 plots did not contain a non-ground LAS return (i.e. HAG > 0) from the thinned 2018 survey. As the majority of these plots contained a non-ground return from the original 2018 point cloud before thinning, this can be attributed to sampling error due to the artificially lower return density. This is supported by the conclusions around lower return densities causing LiDAR pulses to potentially miss individual shrubs in Streuker & Glenn (2006). 114 of the plots were dominated by willow shrubs, 27 by dwarf birch shrubs, and 3 plots were primarily covered with dead shrubs. All direct vegetation height measurements from the

field surveys are found in Table A.2. Maximum LAS return heights within field survey plots from the point clouds are in Table A.3.

The original high-density 2018 point cloud performed well when estimating maximum field-measured plot heights, with an average underestimation of only 10% of total vegetation height and an adjusted R-squared of 0.80 (Table 3.2). The accuracy of LiDAR vegetation height estimation varied across and within the vegetation classes in terms of average proportional underestimation and R^2 (Table 3.2). Maximum heights from the willow shrub class had the strongest correlation with LiDAR return heights, with an average underestimation of only 9.5% and an R^2 of 0.81. Birch heights had a much lower R^2 of 0.61 and greater mean underestimation of 12.3%. The poor performance of the LiDAR when estimating birch heights compared to the other shrub classes could be due to their lower average plot heights of 1.11 m compared to willow shrubs at 1.51 m (Table A.2), but this does not explain their larger proportional underestimations. P-values indicate no correlation between field and LiDAR heights in plots where only non-shrub vegetation was present. This lack of any correlation in plots containing only non-shrub vegetation such as tall grasses was expected due to the lack of standing biomass that would generate a LiDAR return within them, which is supported by the findings of Hopkinson et al. (2005) when comparing grass and herb heights to LiDAR estimates.

Table 3.2: Original 2018 LAS return heights minus field-measured vegetation height metrics within 1 m radius field survey plots

	Vegetation class				
	All plots	All shrubs	Willow	Birch	Grass/moss
Maximum field height					
Mean difference	-0.14	-0.14	-0.14	-0.14	0.07
Mean difference (% of total)	-10.0	-10.0	-9.5	-12.3	-24.7
RMSE	0.32	0.32	0.32	0.34	0.13
R^2	0.80	0.79	0.81	0.61	0.01
p-value	< 0.01	< 0.01	< 0.01	< 0.01	0.82
Average field height					
Mean difference	0.41	0.42	0.43	0.35	0.06
Mean difference (% of total)	48.1	48.1	46.8	56.3	39.3
RMSE	0.55	0.55	0.55	0.27	0.11
R^2	0.69	0.68	0.71	0.56	0.08
p-value	< 0.01	< 0.01	< 0.01	< 0.01	0.95
N	145	142	114	27	3

As more open canopy structures can lead to increased foliage penetration of LiDAR pulses before they generate a return (Hopkinson et al., 2005), the increase in R^2 from 0.80 to 0.85 when comparing maximum heights in plots with over 50% shrub cover using the original 2018 point cloud was expected. When only comparing LiDAR heights to plots with an average field-measured height >= 0.45 m (~2007 LiDAR accuracy RMSE on vegetation points, N = 114), the average underestimation slightly decreased from 10% to 9.1% with an unchanged R^2 of 0.80. This suggests that the amount of shrub cover and canopy structure has a greater influence on the accuracy of height estimations than vegetation height alone.

The original point cloud also drastically overestimates the average field-measured plot heights, with an average overestimation of over 48% and R^2 value dropping to 0.69 when considering all vegetation classes. The vast majority of average plot heights are overestimated by the LiDAR, as seen by the 1:1 line in Figure 3.1. The relation between LiDAR return height and field-measured vegetation heights are stronger than in other studies estimating shrub heights (Estornell et al., 2011;

Hopkinson et al., 2005; Streuker & Glenn, 2006). However, the LiDAR surveys in these previous studies had lower return densities (8/m^2, ~3/m^2, and 1.2/m^2, respectively) than the 11.9 returns/m^2 used here and sensor accuracies have improved over time.

3.2.2 Influence of Return Density

The relationships between field-measured plot heights and LAS return heights are much weaker after thinning the point cloud to match the 2007 return density of 0.67 returns/m^2 (Table 3.3, Figure 3.1). For all vegetation classes under consideration, maximum field-measured plot heights were underestimated by 62.6% on average with an R^2 of 0.55 when compared to LAS return heights from the thinned 2018 point cloud. As with the original point cloud, the lowest average underestimation of 60.6% and highest R^2 of 0.59 were found when only considering the willow shrub class. The LAS return heights did not show a significant relationship with maximum field heights from the birch and non-shrub vegetation classes. Figure 3.1 shows that only one of the plots had a greater LAS return height than measured in the field, with an underestimated slope coefficient of 0.87 from the regression line equation. Though the large number of plots without a non-ground return after thinning would strongly contribute to the overall height underestimations, the non-ground LAS heights in the vast majority of plots are still much lower than the maximum field vegetation heights.

Table 3.3: Thinned 2018 LAS return heights minus field-measured vegetation height metrics within 1 m radius field survey plots

	Vegetation class				
	All plots	All shrubs	Willow	Birch	Grass/moss
Maximum field height					
Mean difference	-0.89	-0.90	-0.91	-0.84	-0.21
Mean difference (% of total)	-62.8	-62.7	-60.6	-0.76	-77.8
RMSE	1.01	1.02	1.03	0.97	0.22
R^2	0.55	0.56	0.59	0.13	0.01
p-value	< 0.01	< 0.01	< 0.01	0.06	0.99
Average field height					
Mean difference	-0.33	-0.34	-0.33	-0.35	-0.09
Mean difference (% of total)	-38.7	-38.6	-36.1	-0.56	-58.9
RMSE	0.54	0.54	0.55	51.0	0.10
R^2	0.64	0.64	0.66	0.33	0.03
p-value	< 0.01	< 0.01	< 0.01	< 0.01	0.89
N	139	136	108	27	3

The lower-density point cloud performs better when comparing to the average heights measured within the plots instead of the maximum heights, as noted in Hopkinson et al. (2005). The LAS return heights are much more distributed around the 1:1 line when compared to average field heights, with a linear regression slope coefficient of 1.04 (Figure 3.1). Average vegetation heights measured within the field plots were underestimated by 38.7%, with an increased R^2 of 0.64. This value did not increase when only considering plots where the majority of their area was covered by shrub vegetation. The best estimations of average field heights are again when only considering willow shrubs, with an average underestimation of 36.1% and an R^2 of 0.55. Birch shrubs consistently perform worse with an average underestimation of 56% and a much lower R^2 of 0.33, which is a greater difference compared to willow shrubs than when using the original2018 point cloud. Only the non-shrub vegetation average heights were found to not have a significant statistical relationship with LAS return heights.

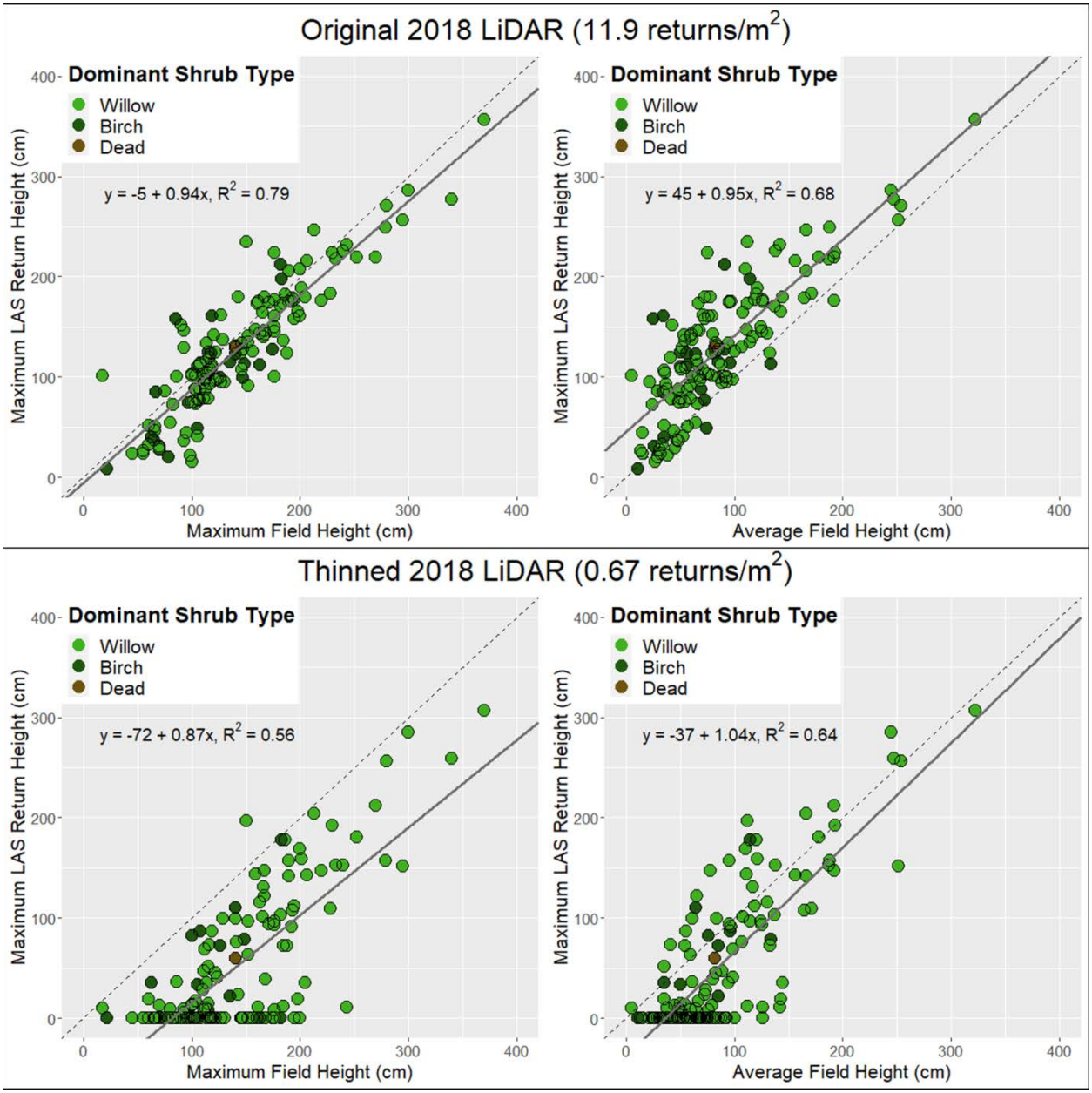

Figure 3.1: LAS return heights from the original and thinned 2018 point clouds within shrub vegetation survey plots compared to field height measurements. The dashed line represents a 1:1 relationship between field and LiDAR heights.

When comparing LiDAR heights to average field-measured heights from plots that still contained a non-ground return after thinning (N = 84), the average percent underestimation decreased from 39% to 16% with an unchanged R^2 of 0.64. If only plots with an average plot height >= 0.45 m were considered, the average underestimation slightly decreased to 36%, but the R^2 also decreased to

0.62 which is consistent with the original point cloud. There was a negligible difference in accuracy when considering plots with an estimated shrub cover greater than or equal to 50% of the total plot area, which was found to improve R^2 in the original point cloud. This supports the conclusion that sampling error from removal of vegetation returns strongly contributed to the decrease in accuracy post-thinning, but does not explain all of the variation.

The original goal of this project was to compare changes in shrub height across Granger Basin between the survey years. However, due to the reduced accuracy of height comparisons after thinning the 2018 LiDAR down to the 2007 return density, the decision was made to focus on the expansion of shrub-covered area between surveys. When considering the large average proportional underestimation compared to field heights using the thinned 2018 point cloud in Table 3.3, it was determined that this would not be feasible for accurately computing changes between it and the 2007 survey. As the HAG metrics from the original high-density 2018 point cloud (11.9 returns/m^2) correlated well with the field height measures (R^2 = 0.79 when compared to maximum plot heights in Table 3.2), height comparisons between LiDAR surveys should be possible with surveys of appropriate return densities and positional accuracies.

3.2.3 Influence of Ground Classification

The selection of ground segmentation algorithms and their respective parameter settings had a strong influence on estimated shrub heights from the LiDAR. Removing vegetation from the ground surface without erasing topography was challenging, slightly more so with the 2007 dataset. The original plan for choosing the final ground segmentation algorithm was to compare RMSE values of fixed-return dGPS points from the vegetation set to ground return elevations. However, this did not appear to influence whether vegetation was included as part of the ground surface or not as interpreted from shaded relief maps created from ground-classified returns (Figure 3.2). Final

decisions were therefore made qualitatively by striking a balance between how well vegetation was removed from the ground surface and preservation of topography. Though using more aggressive parameters successfully removed all visible vegetation in the bare-earth DEM, LAS returns over some of areas of complex topography (ridges/hills/etc.) were not classified as the ground surface which artificially inflated plot HAG values and the amount of shrub-classified pixels over both years.

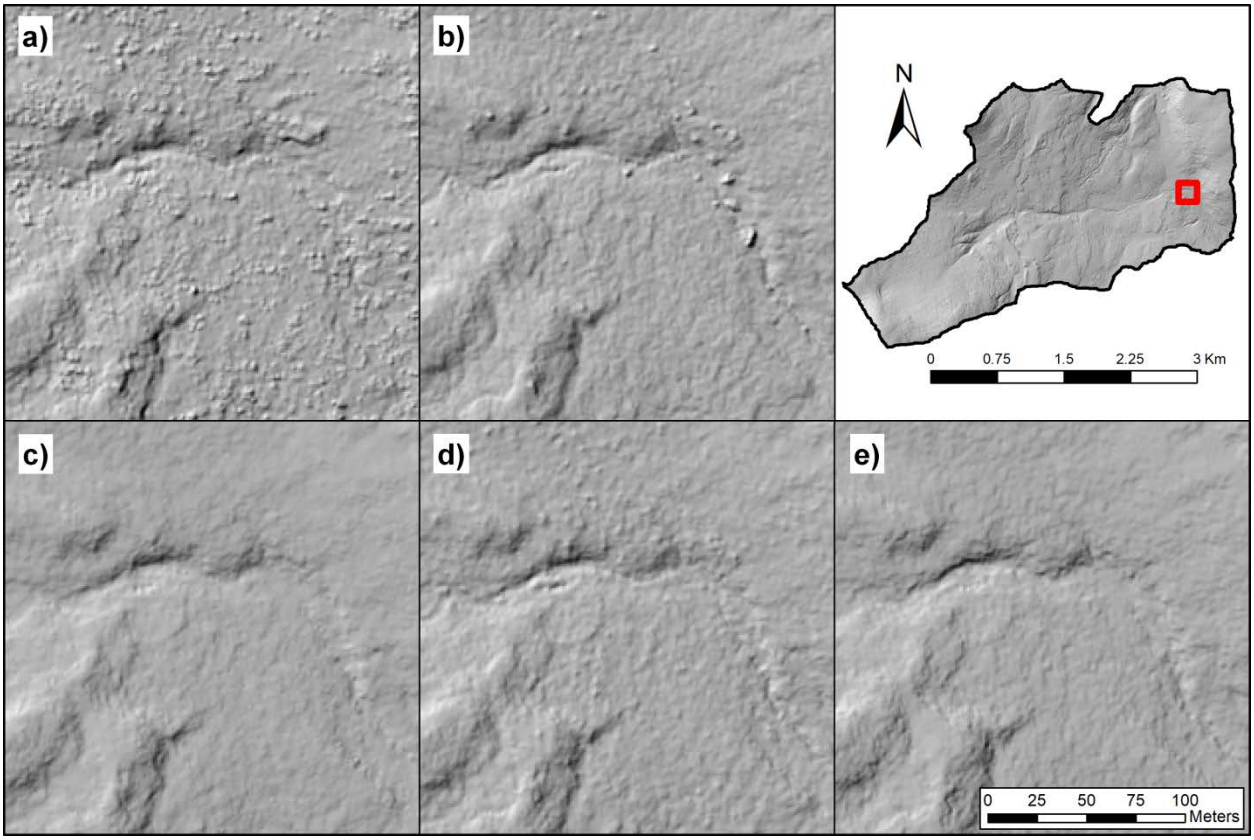

Figure 3.2: Shaded relief maps of Granger Basin, interpolated from ground-returns classified using different algorithms from the thinned 2018 LiDAR. All hillshades were derived from bare-earth DEMs interpolated using a 2nd power IDW with 10 nearest neighbours at a 1 m spatial resolution. The ground segmentation algorithms used in each panel are: a) CSF (Zhang et al., 2016; Roussel & Auty, 2019); b) PMF (Zhang et al., 2003; Roussel & Auty, 2019); c) lasground, more aggressive parameter settings (Axelson, 2000; Isenburg, 2019); d) lasground, less aggressive settings; e) lasground, final parameter combination used.

3.3 Shrub Cover Changes

3.3.1 Variable Reduction

As all 9 HAG- or INT-based rasterized LiDAR metrics for the thinned 2018 point cloud were highly correlated (>0.98), the decision was made to only include one HAG-based metric (ratio of above-cutoff LAS returns to ground returns, or dns) and one intensity metric (maximum intensity recorded by the returns, or maxINT) along with elevation for use in the final shrub classifications. Though dns and maxINT remain highly correlated, both of these rasterized LiDAR metrics were included as predictor variables as they represent different physical processes of LAS return height and return strength, respectively.

3.3.2 Overall Change

When running the 25 seed iterations, the RF classifications resulted in a slightly higher average overall accuracy (93.1% vs. 92.7%) and kappa coefficient (0.86 vs. 0.85), with a smaller range between the minimum and maximum area classified as shrub (0.51 km^2 vs. 0.63 km^2) than when using SVM (see section 2.6.2 description of methods). The overall independent accuracy from the validation set, kappa coefficient, and stability of shrub-classified area presented in Table A.4 were all considered when selecting the final classification. The RF classification with highest independent accuracy (using seed 15 to sample training and validation sets) was applied to the 2018 and 2007 point clouds and evaluate change between those years.

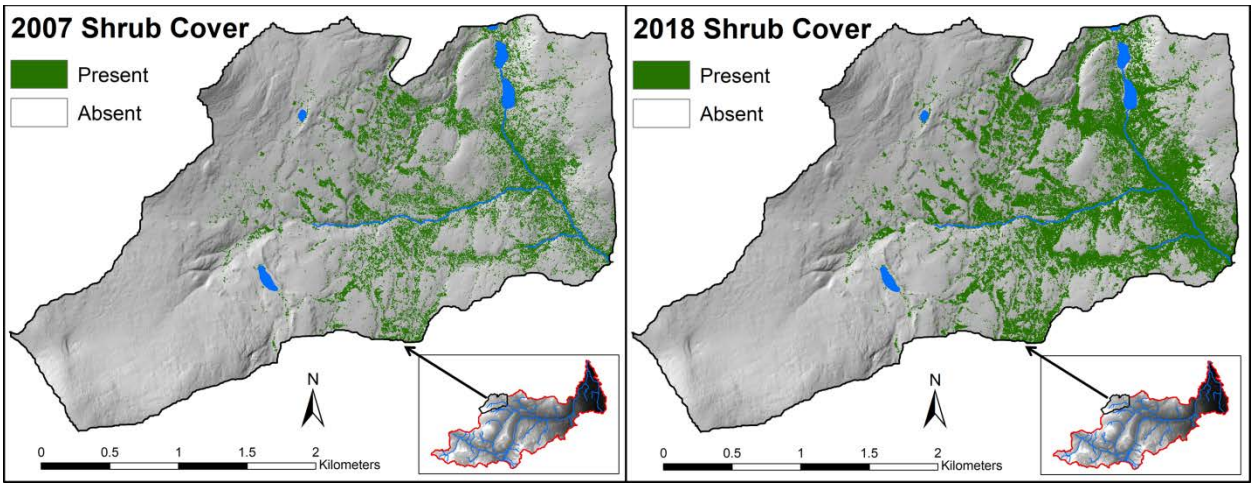

Figure 3.3: Best-performing classifications of detectable shrub cover > 45 cm in height within Granger Basin generated using 2007 and 2018 LiDAR metrics

After the removal of pixels above the shrubline and within lake extents, the best-performing RF classifications (with 97.1% overall independent accuracy) gave 1.60 km^2 of total shrubbed area with heights greater than 0.45 m in 2018 compared to 0.98 km^2 in 2007; an overall increase of 63.3% (Figure 3.2). In terms of areal coverage, 0.77 km^2 of Granger Basin showed an increase in shrub cover with 0.15 km^2 of loss. Stable shrubs (i.e. pixels with a value of 1 in both classifications) as seen in Figure 3.3 had an area of 0.83 km^2, while areas of stable non-shrub made up 5.41 km^2.

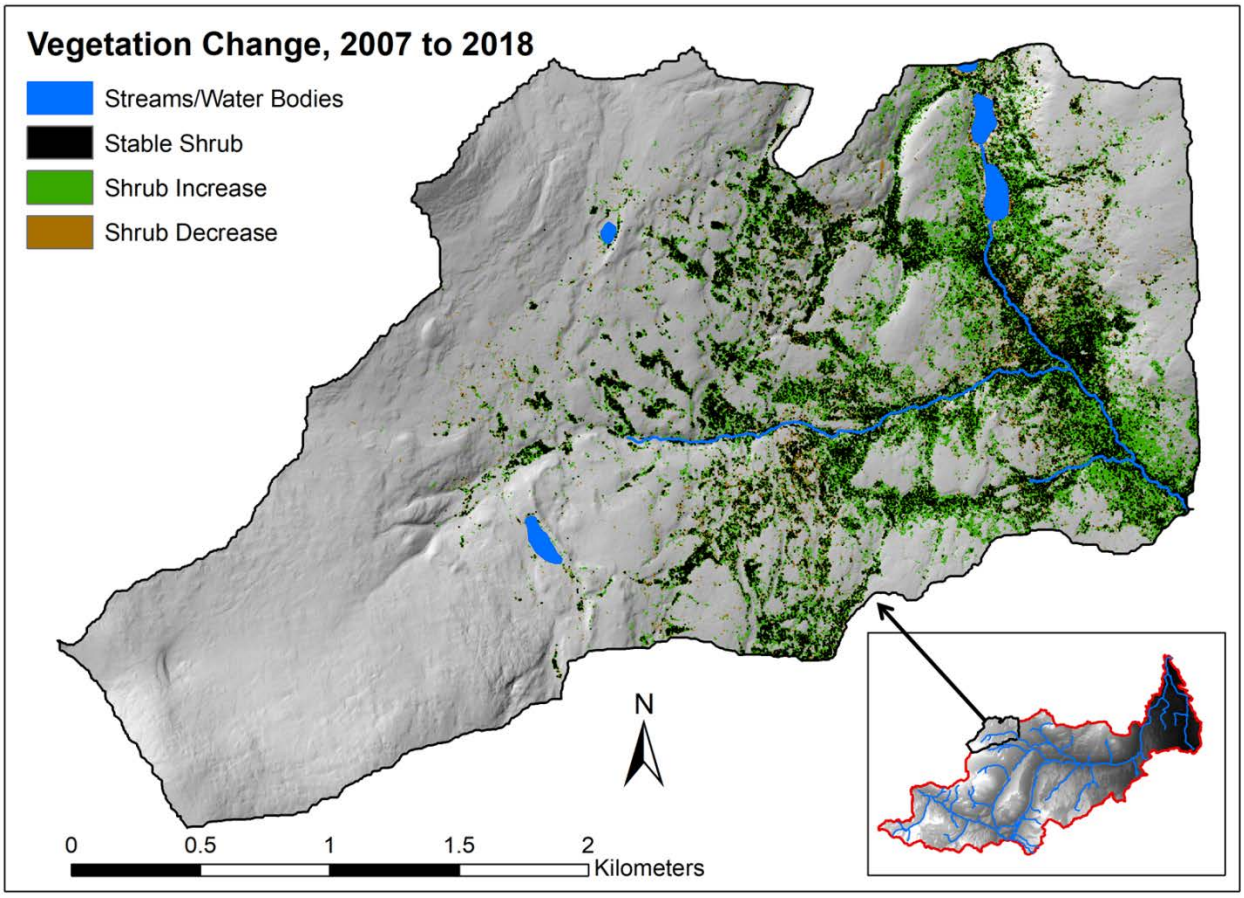

Figure 3.4: Changes in detectable shrub cover > 45 cm in height within Granger Basin between 2007 and 2018, separated into categories used for terrain derivative comparisons

The average yearly increase in shrub cover of 5.8% in Granger Basin is greater than what has been reported in previous works that quantify the expansion of shrub and woody vegetation in northern regions (Naito & Cairns, 2011a; Tape et al., 2006; Tape et al., 2012; Tremblay et al., 2012). Studies examining shrub expansion in northern Alaska and eastern Nunavik using historical and repeated airphotos along with high-resolution satellite imagery have found large amounts of regional variation in the rates of increasing vegetation cover, with maximum documented rates that are comparable to this study. In the Brooks Range and Northern Slope uplands of Alaska (with latitudes of 68 – 69 ºN), Naito & Cairns (2011a) and Tape et al. (2006) found maximum yearly increases in shrub cover of 3.5% and 2.5% respectively when only considering patches located within terraces and floodplain areas, which are comparable to the 5.8% annual increase found in this study. Overall

increases when averaged over all repeated airphotos analyzed were typically much lower than the maximum rates found in higher-resource areas such as floodplains, terraces, and riparian zones, which could be due to the wide geographic coverage and resulting range of climate and topography of the study areas (Naito & Cairns, 2011a; Tape et al., 2006). While Tremblay et al. (2012) examined changes in shrub and tree cover over environmental parameter classes at a similar latitude (58 ºN) and over a similar area (~6 km^2) as Granger Basin, the maximum annual increase in continuous cover of 2.7% and average of 0.8% are much lower than found in this study. A potential contributor to lower annual expansion rates in the "erect woody vegetation" class used is the inclusion of trees along with shrubs, due to their relatively slower rates of areal expansion compared to shrub vegetation (Epstein et al., 2013).

The majority of these previous works focus on longer-term changes (45 – 60 years) in Arctic tundra environments located at higher latitudes (>68 ºN) than considered in this work. The increased productivity of Granger Basin due to a lower latitude of 60 ºN and warmer continental subarctic climate may contribute to the increased magnitude of yearly vegetation change when compared to other studies. Another possible explanation for these differences is the increased rate of climate warming and resulting change in environmental properties in more recent years (Dillon et al., 2010).

3.3.3 Classification Sensitivity

All accuracies and total shrub-classified areas presented in Table A.4 predicted using the thinned 2018 LiDAR varied widely depending on the random seed set for splitting points into the training and validation sets. Over the 25 classifications for each algorithm, overall accuracies varied by 10.29% with RF and 11.76% with SVM, while the amount of shrub-classified area varied by 0.51 km^2 and 0.63 km^2 respectively. With only a 0.41% difference in average accuracy between RF and SVM, the differences in accuracy between classification iterations was much more sensitive to which

points were used for training and validation than the algorithm used to classify them. Class stabilities varied slightly more than accuracy over the RF and SVM algorithms, but were also much more sensitive to seed selection. There were identical differences in the minimum and average amounts of shrub-classified area produced by the classifiers at 0.1 km^2, and only a 0.01 km^2 difference in the maximum.

The variation in shrubbed area could be due to different characteristics of points used to train the classifiers. As the average shrub heights measured in the 114 plots used as detectable shrub presence points ranged from 0.45 m to 3.22 m, a large range of predictor variable values would be captured when training the models and validating the resulting classifications. As shrubs with lower heights and canopy densities may not be captured by the LiDAR and therefore the derived predictor variable rasters (Hopkinson et al., 2005; Streuker & Glenn, 2006), the inclusion of more of these points in the validation set could lead to lower accuracies. Conversely, if a larger proportion of these presence points with lower heights and densities were used to train the models, this could lead to overestimation of shrub cover. This is supported by identical minimum accuracies of 86.8% and only a 1.5% difference between the maximum accuracies between RF and SVM.

3.4 Landscape-Scale Variation

3.4.1 Statistical Differences in Shrub Distribution

The terrain derivatives with the strongest relationships according to Spearman's rank correlation test were all measures of distance to stream (Euclidean, vertical, overland flow) with the minimum level of correlation being 0.86 between vertical and overland, which is expected. All stream distance measures were also highly correlated with elevation as the interconnected stream network exists within the lower basin, with overland flow being the least correlated with elevation at

0.84. Due to these relationships between stream distance metrics, only horizontal overland flow was retained for use as it was less strongly correlated to other terrain indices under consideration.

The Wilcoxon rank-sum test results presented in Table 3.4 show that for all terrain derivatives explored, stable and expanding shrub pixels are preferentially located in areas that fulfill the alternative hypotheses used when compared to the other change classes in a pairwise manner. An alternative hypothesis of “lesser” tests whether the value distribution of a numeric vector is lower than another that it is being compared to, while the opposite is true when using the “greater” alternative hypothesis. Elevation values in pixels exhibiting an increase in shrub cover were lower than areas of stable shrub, shrub loss, stable non-shrub, and the overall Granger basin. For the slope gradient, northness, stream distance, and relative slope position, the value distributions of the stable shrub pixels were lower than the shrub gain pixels, which were then lower than each of the other classes. Shrub loss pixels also had more preferential terrain derivative values than areas of stable non-shrub or Granger Basin in all instances. For example, the SWI and northness value distributions in the shrub loss category were lower than in the stable shrub or gain pixels, but greater than in the stable non-shrub or the overall Granger Basin categories. These results indicate that shrubs in Granger Basin are found in and are preferentially expanding into lower and flatter areas near stream networks, with lower slope positions and a higher potential for topographic wetness.

Table 3.4: Summary of results from Wilcoxon rank-sum tests, used to explore where stable and expanding shrub pixels are preferentially located according to terrain derivative value distributions

Landscape property	**Alternative hypothesis**	**Value distributions per change category**
Elevation	Less	Gain pixels < stable shrub, loss, stable non-shrub, Granger (overall)
		Stable shrub pixels < loss, stable non-shrub, Granger (overall)
Slope gradient	Less	Gain pixels < loss*, stable non-shrub, Granger (overall)
		Stable shrub pixels < gain, loss, stable non-shrub, Granger (overall)
Northness	Less	Gain pixels < stable non-shrub, Granger (overall)
		Stable shrub pixels < gain, stable non-shrub, Granger (overall)
Eastness	Greater	Gain pixels > stable non-shrub, Granger (overall)
		Stable shrub pixels > gain, loss, stable non-shrub, Granger (overall)
Stream distance (overland flow)	Less	Gain pixels < loss, stable non-shrub, Granger (overall)
		Stable shrub pixels < gain, loss, stable non-shrub, Granger (overall)
SAGA wetness index	Greater	Gain pixels > loss, stable non-shrub, Granger (overall)
		Stable shrub pixels > gain, loss, stable non-shrub, Granger (overall)
Relative slope position	Less	Gain pixels < loss, stable non-shrub, Granger (overall)
		Stable shrub pixels < gain, loss, stable non-shrub, Granger (overall)

* indicates $p < 0.05$, all other p-values < 0.01

For every terrain derivative other than elevation, the stable shrub pixels had greater differences in terrain values than the expanding shrub class when compared to the loss or stable shrub classes. Values from the shrub loss class were also closer to the gain and stable shrub than the stable non-shrub or overall Granger classes in all cases. This is contrary to what Naito & Cairns (2011a) found when comparing shrub change classes over ranges of topographic wetness values, and some of the findings from Tape et al. (2006) when exploring landscape positions of stable and expanding patches. As productivity is already high in lowland environments and riparian zones, vegetation in these areas may be less responsive to warming (Campbell et al., 2020). Tape et al. (2006) found that stable shrub patches occupied broader and less-sloping landscape positions than expanding patches, which could explain these results in terms of slope gradient and position.

Although climatic warming is believed to be the dominant broad-scale driver of Arctic vegetation change, the processes underlying finer-scale increases are unclear due to the wide range of

contributing environmental changes (Tape et al., 2012; Tremblay et al., 2012). This expansion is driven by the interaction of temperature, nutrient cycling, decomposition, and soil conditions (Naito & Cairns, 2011b; Tape et al., 2012). The preferential location of expanding and stable shrub pixels in areas of lower elevation, lower slope gradient and position, higher topographic wetness, and higher stream proximity are all consistent with previous findings and supported by established physical processes (Tape et al., 2006; Naito & Cairns, 2011a; Tremblay et al., 2012).

As slopes in arctic and subarctic environments tend to represent a gradient of climate, nutrient and moisture availability, their influence on environmental phenomena such as soil drainage, depth, and snow accumulation result in vegetation patterns that are strongly correlated with relief (Walker, 2006). The association of high SWI values with positive changes in Arctic shrub cover can be explained by its determination of nutrition resources with an overwhelming influence on the distribution of woody plants (Wu & Archer, 2005; Walker, 2006; Naito & Cairns, 2011a). Riparian areas with preferential water flow are similarly higher-resource environments, which would explain the preferential location of stable and expanding shrub pixels closer to the stream network (Myers-Smith et al., 2011; Naito & Cairns, 2011a; Tape et al., 2012). The elevation range of ~725 m.a.s.l. within Granger Basin results in a gradient of climatic and hydrometeorological conditions (McCartney et al., 2006), which would contribute to the large contrast between shrub change categories across the elevation classes.

3.4.2 Categorical Comparisons

These changes were further explored by comparing the percentage of total pixels in each shrub change category falling into individual terrain derivative value classes (Table 3.5). This further illustrates how much of a difference in terrain value distribution exists between areas of stable shrubs and increasing shrubs compared to the overall Granger Basin. As with the Wilcoxon tests, the stable

shrub pixels have the largest difference in terrain value distributions compared to Granger Basin overall area, followed by areas of increasing and then decreasing shrub presence. For example, while only 31.9% of Granger Basin is within 500 m of the stream network (according to overland flow), 63.7% and 66.6% of the stable shrub and increasing shrub areas respectively are within this distance class. This same relationship is seen in the elevation values, with 31.1% of stable shrub pixels located < 1450 m.a.s.l. compared to 10.2% of the study area. A smaller but notable difference exists when examining the lowest slope gradient class of 0-5 º, with stable shrub and overall Granger areal percentages of 32% and 18.5% respectively. Conversely, while 38.8% of Granger Basin has a relative slope position of >0.85 (i.e. closer to the tops of ridges), only 15.4% of the increasing shrub pixels are located in these areas. Stable and expanding shrub areas are also preferentially located in areas of high topographic wetness, with 37.7% and 24.8% of these pixels having SWI values within the 2 highest categories (>5) compared to only 12.7% of the overall Granger Basin. Though tundra shrubline advance in Yukon's Kluane Region was not found to be influenced by slope aspect (Myers-Smith & Hik, 2018), Tremblay et al. (2012) found that increases in standing woody vegetation cover at a similar latitude to Granger Basin occurred mainly on south-facing slopes. The Wilcoxon tests show that value distributions of stable and expanding shrub pixels have statistically higher eastness and lower northness when compared to the other classes, but there does not appear to be much difference based on cardinal direction in Table 3.5.The largest differences over the terrain derivative value classes are in stream distance, elevation, and relative slope position.

Table 3.5: Changes in shrub cover compared over different value classes for selected terrain derivatives, represented by the percentage of total pixels within category

	Shrub change category			
	Stable Shrub	**Increase**	**Decrease**	**Granger (Overall)**
Overall Coverage	11.6	10.8	2.2	100
Elevation (m.a.s.l.)				
1300-1450	31.1	27.9	22.2	10.2
1450-1600	65.1	67.3	67.2	46.5
1600-1750	3.8	4.8	10.5	27.5
1750-1900	0	0	0	9.4
>1900	0	0	0	6.4
Slope aspect				
N	23.3	23.7	20.9	22.3
E	21.4	23.8	26	23.7
S	19.5	20.7	23.2	22.6
W	24.3	24.2	22.1	25.3
Flat (slope <= 3 º)	11.4	7.6	7.8	6
Slope gradient (º)				
0-5	32	23	22.7	18.5
5-10	41.8	39.7	39.8	36.1
10-15	15.9	19.9	20.6	22.3
15-25	9	14.9	13.6	19.9
>25	1.3	2.4	3.4	3.2
Overland flow distance to stream (m)				
0-500	63.7	66.6	53.7	31.9
500-1000	15.8	16.8	22.1	21.4
1000-1500	15.6	11.9	18.1	20
1500-2000	4.6	4.2	5.4	15.6
>2000	0.2	0.4	0.7	11.1
SAGA wetness index				
0-3	0.5	1.6	1.8	6
3-4	11.9	24.5	24.1	37.7
4-5	49.8	49.1	55	43.7
5-6	25.4	18.7	15.5	9.9
>6	12.3	6.1	3.6	2.8
Relative slope position				
0-0.15	55.3	50.3	41.8	28.3
0.15-0.4	14.9	15.7	14.8	12.2
0.4-0.6	7	8.2	9.4	7.9
0.6-0.85	9.4	10.4	13	12.8
>0.85	13.4	15.4	21	38.8

3.5 Implications for Granger Basin

As the presence of tall shrub patches can substantially modify the local environment in taiga-tundra ecozones, the rapid rate of shrub expansion within Granger Basin has a wide range of implications for the hydrological processes of the study area (Wallace & Baltzer, 2019). The impacts of increased shrub cover on the exchange of energy among the atmosphere, vegetation, and soils of Granger Basin are varied due to interactions between shrub canopies and snow cover (Myers-Smith et al., 2011). Due to the increased aerodynamic roughness of exposed shrubs, a greater amount of canopy coverage will lead to increased snow storage in Granger Basin (Essery et al., 2006; Pomeroy et al., 2006). The insulative effects of wind-compacted snow layers trapped under tall shrub canopies can lead to winter soil temperatures being up to 30 ºC greater than air temperatures (Sturm et al., 2001b). Due to resulting shallower thaw depths and increased melt rates, the large proportional expansion of shrubs at lower elevations will impact the response of the discontinuous permafrost within Granger Basin to warming (Essery et al., 2006; Lawrence & Swenson, 2011; McCartney et al., 2006; Pomeroy et al., 2006). Though the specific influences of shrub expansion on permafrost vulnerability are complex, an increase in thawing would impact groundwater and hydrological responses to change (Bonfils et al., 2012; Carey et al., 2013).

Shifts in Arctic and subarctic vegetation under future warming are projected to have an overall positive feedback to climate due to changes in the energy balance (Pearson et al., 2013). A decrease in albedo and resulting greater summer sensible heat flux due to increased shrub cover will cause a positive atmospheric heating effect (Lafleur & Humphreys, 2018). Evapotranspiration energy is predicted to increase along with shrub vegetation cover, but with a smaller magnitude relative to the effects of albedo (Pearson et al., 2013).This positive feedback on warming will have further cumulative effects on the energy balance and future climate of Granger Basin, as well as other similar northern catchments (Ménard et al., 2014).

Increased rainfall interception is a major component of the water balance in Arctic shrub tundra ecosystems, with effective below-canopy rainfall being reduced by up to 30% under birch canopies (Zwieback et al., 2019). Increased evapotranspiration due to shrub vegetation presence will lead to an increased uptake of snowmelt water compared to precipitation used in the summers, as found at a similar shrub taiga site within the WCRB (Granger, 1999). Greater transpiration rates from shrub cover may also increase atmospheric water vapour concentrations (Bonfils et al., 2012). On larger scales, the increased rainfall interception of shrub canopies reduces water yield, which in term would decrease the amount of runoff received by downstream ecosystems (Zwieback et al., 2019). However, a disproportionate amount of runoff was computed from tall shrub hydrological response units in Granger Basin by McCartney et al. (2006), which would be expected to continue with over 21% of the study area covered by shrubs > 0.45 m in height in 2018 compared to ~13% in 2007.

The expansion of shrub vegetation into Arctic streams and in floodplain areas will likely lead to changes in streamflow pathways and water quality across the lower Granger Basin (Tetzlaff et al., 2013). The effects of increased riparian vegetation on microclimatic variables and energy inputs due to shading of the water column have a variety of influences on stream temperature, with changes in vegetation density and height potentially buffering climate change effects (Fabris et al., 2020; Garner et al., 2017). Interactions between climate and soils along with vegetation community composition will have complex influences on the dynamics of dissolved organic matter within the lakes and streams of Granger Basin and the larger WCRB (Shatilla & Carey, 2019). The increase in tall shrubs has contributed to a decline in erosion in Arctic floodplains, along with an increase in stabilized soil and nitrogen mineralization rates (Myers-Smith et al., 2011; Tape et al., 2011). Carbon cycling rates are also enhanced under greater shrub cover, with greater seasonal net CO_2 sinks resulting in negative feedback to the atmosphere (Lafleur & Humphreys; 2018).

3.6 Limitations & Areas for Future Research

Due to the 2 m spatial resolution of the rasterized LiDAR metrics required by the lower-density point clouds, this study was unable to distinguish between the different types of shrub expansion proposed by Tape et al. (2006). The use of binary shrub and non-shrub classifications removes any potential for evaluating changes in vegetation properties other than cover over time, as LiDAR vegetation height estimates were found to be too inaccurate to compare across surveys. This study also only considers taller shrubs that are >0.45 m in height within the classifications due to the limits on the 2007 LiDAR accuracy in steeper and more vegetated terrain. Another potential issue is the lack of validation data collected around the 2007 LiDAR survey leading to the inability to assess the accuracy of the 2007 shrub classification. Though LiDAR resolutions were standardized to mitigate return density bias, potential differences in point cloud structure due to sensor configurations and acquisition parameters could lead to shrubs showing different signatures within the 2007 and 2018 LiDAR-derived predictor metrics. Future studies with longer-term planning should use coincident field vegetation surveys along with each LiDAR acquisition flight to ensure that shrub metrics for each year under consideration have the best possible resemblance to reality. The LiDAR instruments used, acquisition parameters, and flight conditions should also be as similar as possible to reduce any potential bias between surveys. As Hopkinson et al. (2008) found that a 10% uncertainty in conifer plantation growth estimates could be achieved at a 3-year time interval between LiDAR surveys, a similar interval could feasibly capture shrub changes within Granger Basin due to the large annual expansion rate found in this study. However, the higher proportional LiDAR height underestimation and greater expansion rates relative to trees may lead to differences in the minimum return interval required for accurately measuring changes in lower-stature vegetation (Epstein et al., 2013; Estornell et al., 2011; Greaves et al., 2016; Hopkinson et al., 2005; Streuker & Glenn, 2006).

Greaves et al. (2016) used canopy metrics derived from high-resolution LiDAR and multispectral imagery to predict shrub biomass with high accuracy, while lower-resolution LiDAR has also been used to estimate fractional vegetation cover in forest ecozones (Hopkinson & Chasmer, 2009). With the advances of higher-resolution drone-mounted LiDAR sensors in recent years, their documented uses for forestry practices could potentially carry over to lower-stature shrub vegetation (Kellner et al., 2019). The inclusion of high-resolution multispectral imagery and photogrammetric point clouds from UAV sensors is another option that could pair well with the high-density 2018 LiDAR, but is limited by lower areal coverage per survey than plane-mounted LiDAR instruments and potential issues with reproducibility due to varying deployment conditions (Harder et al., 2016). Coincident plane-mounted LiDAR and photogrammetric point clouds from UAV surveys have been used in the past to evaluate change in forestry metrics, with varying levels of accuracy depending on vegetation properties (Ali-Sisto & Petteri, 2017). A possibility to explore is the feasibility of quantifying shrub changes in Granger Basin by using airborne LiDAR to derive an accurate bare-ground terrain surface, matched with high-resolution photogrammetric point clouds from UAV surveys to provide information on the shrub canopy above this surface. With increased LiDAR survey resolutions, better standardization between acquisitions, and the incorporation of other high-resolution remotely sensed imagery, object-based classifications or regression models could potentially distinguish between in-filling, increasing shrub size, and new colonization, as well as measure changes in vegetation properties other than cover over time (Lantz et al., 2010; Myers-Smith et al., 2011; Greaves et al., 2016).

CHAPTER 4: SUMMARY & CONCLUSIONS

High-latitude ecosystems have experienced substantial warming over the past 40 years, causing an increase in vegetation growth throughout the circumpolar North (Hinzman et al., 2005; Overpeck et al., 1997; Sturm et al., 2001a; Tape et al., 2006). A major component of this change is shrub expansion in arctic and subarctic ecotones (Tape et al., 2006; Epstein et al., 2013; Myers-Smith et al., 2011). The rates of shrub expansion are highly variable depending on plant species, topographic position, hydrology, soils, and other ecosystem properties (Naito & Cairns, 2011a; Tape et al., 2012). Such changes in shrubs and other vegetation are critical to document due to their first-order control on water, energy, and carbon balances. This study has used multi-temporal LiDAR along with field vegetation surveys to evaluate shrub expansion between 2007 and 2018 in a well-studied subarctic mountain basin, and quantitatively compared how changes in vegetation cover varied over a range of landscape properties.

The original goal of this research was to compare changes in shrub height across the ~7.6 km^2 Granger Basin between LiDAR surveys. The high-resolution 2018 point cloud was found to estimate field-measured vegetation heights with reasonable accuracy, but the resulting large proportional height underestimation after standardizing return density to 2007 levels would not be feasible for accurately comparing changes. A decision was therefore made to evaluate changes in shrub cover using binary presence and absence models, created through machine learning classifications based on rasterized LiDAR metrics. The best-performing shrub classifications created using the random forests algorithm showed a 63.3% increase in total detectable cover > 0.45 m in height between 2007 and 2018, a 5.8% average yearly increase. This average annual expansion rate is greater than what has been previously found in the literature (Naito & Cairns, 2011a; Tape et al., 2006; Tape et al., 2012; Tremblay et al., 2012), which

could be explained by the lower latitude, warmer climate, and resulting higher productivity of Granger Basin when compared to the Arctic tundra sites studied in previous works.

Value distributions of several terrain derivatives were compared to examine landscape-scale variation between areas of shrub gain, stable shrub, shrub loss, stable non-shrub, and the overall Granger Basin. Wilcoxon rank-sum tests found statistical differences in elevation, slope gradient, northness, eastness, stream distance, topographic wetness, and relative slope position values between areas of stable and expanding compared to the other change categories. Shrubs were found to be located in and preferentially expanding into lower and flatter areas near stream networks, with lower slope positions and a higher potential for topographic wetness. When stable and expanding shrub pixels were compared to Granger Basin as a whole, the greatest differences in terrain value distributions were found in terms of stream distance, elevation, and relative slope position. The expansion of shrubs into these higher-resource areas is consistent with previous studies and is supported by established physical processes.

This large increase in shrub cover has far-reaching implications for northern freshwater ecology due to the influence of vegetation on water, energy, and carbon balances (Epstein et al., 2013; Lafleur & Humphreys, 2018; Myers-Smith et al., 2011; Tetzlaff et al., 2013). Increased snowmelt rates under shrub canopies due to higher winter soil temperatures have complex effects on the vulnerability of permafrost to warming, which will in turn impact groundwater and streamflow responses. Expansion and densification of shrubs leads to a decrease in albedo and an increase in absorbed solar radiation, contributing to a positive global warming feedback that will further impact similar catchments across the circumpolar North. Increased interception, snow storage, and snowmelt water uptake due to the presence of tall shrubs can lead to substantial increases in runoff volume and contribute to major changes in the overall water balance. The

interactions between climate soils, and vegetation in riparian areas has complex effects on dissolved nutrient dynamics and carbon cycling rates, along with increased shading of the water column contributing to changes in stream temperature.

This study has demonstrated the feasibility of using LiDAR to compare changes in shrub properties over time, though the potential for accurately measuring changes in properties other than cover are limited by return density. Future studies using higher-resolution LiDAR surveys along with coincident optical satellite or UAV imagery could potentially distinguish between the different proposed types of Arctic and subarctic shrub expansion (in-filling, increasing shrub size, and new colonization), as well as measure changes in vegetation properties other than cover over time. A greater understanding of how such changes vary at the landscape scale over different physiographic variables is crucial for predicting the future of northern watersheds under a rapidly changing climate.

REFERENCES

Ali-Sisto, D., & Packalen, P. (2017). Forest Change Detection by Using Point Clouds from Dense Image Matching Together with a LiDAR-Derived Terrain Model. *IEEE Journal of Selected Topics in Applied Earth Observations and Remote Sensing*, *10*(3), 1197–1206. https://doi.org/10.1109/JSTARS.2016.2615099

Applied Geomatics Research Group (2008). IP3 LiDAR collaborative research data report.

Axelsson, P. (1999). Processing of laser scanner data - Algorithms and applications. *ISPRS Journal of Photogrammetry and Remote Sensing*, *54*(2–3), 138–147. https://doi.org/10.1016/S0924-2716(99)00008-8

Axelsson, P. (2000). DEM generation from laser scanner data using adaptive TIN models. *International Archives of Photogrammetry and Remote Sensing*, *33*(4), 110–117. Retrieved from https://www.isprs.org/proceedings/XXXIII/congress/part4/111_XXXIII-part4.pdf

Bater, C. W., Wulder, M. A., Coops, N. C., Nelson, R. F., Hilker, T., & Næsset, E. (2011). Stability of Sample-Based Scanning-LiDAR-Derived Vegetation Metrics for Forest Monitoring. *IEEE Transactions on Geoscience and Remote Sensing*, *49*(6), 2385–2392.

Belgiu, M., & Drăgu, L. (2016). Random forest in remote sensing: A review of applications and future directions. *ISPRS Journal of Photogrammetry and Remote Sensing*, *114*, 24–31. https://doi.org/10.1016/j.isprsjprs.2016.01.011

Beven, K. J., & Kirkby, M. J. (1979). A physically based, variable contributing area model of basin hydrology. *Hydrological Sciences Bulletin*, *24*(1), 43–69. https://doi.org/10.1080/02626667909491834

Blok, D., Heijmans, M. M. P. D., Schaepman-Strub, G., Kononov, A. V., Maximov, T. C., & Berendse, F. (2010). Shrub expansion may reduce summer permafrost thaw in Siberian tundra. *Global Change Biology*, *16*(4), 1296–1305. https://doi.org/10.1111/j.1365-2486.2009.02110.x

Böhner, J., Köthe, R., Conrad, O., Gross, J., Ringeler, A., & Selige, T. (2001). Soil regionalisation by means of terrain analysis and process parameterisation. *European Soil Bureau*, (May 2015), 213–222. Retrieved from http://www.scilands.de/referenzen/veroeffentlichung/601Bohner.pdf

Bollandsås, O. M., Gregoire, T. G., Næsset, E., & Øyen, B. H. (2013). Detection of biomass change in a Norwegian mountain forest area using small footprint airborne laser scanner data. *Statistical Methods and Applications*, *22*(1), 113–129. https://doi.org/10.1007/s10260-012-0220-5

Bonfils, C. J. W., Phillips, T. J., Lawrence, D. M., Cameron-Smith, P., Riley, W. J., & Subin, Z. M. (2012). On the influence of shrub height and expansion on northern high latitude climate. *Environmental Research Letters*, *7*(1), 015503. https://doi.org/10.1088/1748-9326/7/1/015503

Breiman, L. (2001). Random Forests. *Machine Learning*, *45*, 5–32.

Campbell, T. K., F., Lantz, T. C., Fraser, R. H., & Hogan, D. (2020). High Arctic Vegetation Change Mediated by Hydrological Conditions. *Ecosystems*. https://doi.org/10.1007/s10021-020-00506-7

Chasmer, L., Hopkinson, C., Treitz, P., Mccaughey, H., Barr, A., & Black, A. (2008). A lidar-based hierarchical approach for assessing MODIS f PAR. *Remote Sensing of Environment*, *112*(12), 4344–4357. https://doi.org/10.1016/j.rse.2008.08.003

Carey, S. K., Boucher, J. L., & Duarte, C. M. (2013). Inferring groundwater contributions and pathways to streamflow during snowmelt over multiple years in a discontinuous permafrost subarctic environment (Yukon, Canada). *Hydrogeology Journal*, *21*(1), 67–77. https://doi.org/10.1007/s10040-012-0920-9

Cao, L., Coops, N. C., Innes, J. L., Sheppard, S. R. J., Fu, L., Ruan, H., & She, G. (2016). Estimation of forest biomass dynamics in subtropical forests using multi-temporal airborne LiDAR data. *Remote Sensing of Environment*, *178*, 158–171. https://doi.org/10.1016/j.rse.2016.03.012

Cardoso, P. (2020). red: IUCN Redlisting Tools. R package version 1.5.0. https://CRAN.R-project.org/package=red

Carlberg, M., Gao, P., Chen, G., & Zakhor, A. (2009). Classifying urban landscape in aerial lidar using 3D shape analysis. *Proceedings - International Conference on Image Processing, ICIP*, 1701–1704. https://doi.org/10.1109/ICIP.2009.5413385

Castillo, M., Rivard, B., Sánchez-Azofeifa, A., Calvo-Alvarado, J., & Dubayah, R. (2012). LIDAR remote sensing for secondary Tropical Dry Forest identification. *Remote Sensing of Environment*, *121*, 132–143. https://doi.org/10.1016/j.rse.2012.01.012

Congalton, R. G., & Green, K. (2008). Assessing the Accuracy of Remotely Sensed Data. *CRC Press*. https://doi.org/10.1201/9781420055139

Conrad, O., Bechtel, B., Bock, M., Dietrich, H., Fischer, E., Gerlitz, L., Wehberg, J., Wichmann, V., and Boehner, J. (2015): System for Automated Geoscientific Analyses (SAGA) v. 2.1.4. Geosci. Model Dev., 8, 1991-2007, doi:10.5194/gmd-8-1991-2015

Dillon, M. E., Wang, G., & Huey, R. B. (2010). Global metabolic impacts of recent climate warming. *Nature*, *467*(7316), 704–706. https://doi.org/10.1038/nature09407

Duro, D. C., Franklin, S. E., & Dubé, M. G. (2012). A comparison of pixel-based and object-based image analysis with selected machine learning algorithms for the classification of agricultural landscapes using SPOT-5 HRG imagery. *Remote Sensing of Environment*, *118*, 259–272. https://doi.org/10.1016/j.rse.2011.11.020

Epstein, H. E., Raynolds, M. K., Walker, D. A., Bhatt, U. S., Tucker, C. J., & Pinzon, J. E. (2012). Dynamics of aboveground phytomass of the circumpolar Arctic tundra during the past three decades. *Environmental Research Letters*, *7*(1). https://doi.org/10.1088/1748-9326/7/1/015506

Epstein, H. E., Myers-Smith, I., & Walker, D. A. (2013). Recent dynamics of arctic and sub-arctic vegetation. *Environmental Research Letters*, *8*(1). https://doi.org/10.1088/1748-9326/8/1/015040

ESRI (2019). ArcGIS Pro: Release 2.4.2. Redlands, CA: Environmental Systems Research Institute.

Essery, R., Granger, R., & Pomeroy, J. (2006). Boundary-layer growth and advection of heat over snow and soil patches: Modelling and parameterization. *Hydrological Processes*, *20*(4), 953–967. https://doi.org/10.1002/hyp.6122

Estornell, J., Ruiz, L. A., & Veláquez-Marti, B. (2011). Study of Shrub Cover and Height Using LIDAR Data in a Mediterranean Area. *Forest Science*, *57*(3), 171–179. https://doi.org/https://doi.org/10.1093/forestscience/57.3.171

Fabris, L., Rolick, R. L., Kurylyk, B. L., & Carey, S. K. (2020). Characterization of contrasting flow and thermal regimes in two adjacent subarctic alpine headwaters in Northwest Canada. *Hydrological Processes*, 1–19. https://doi.org/10.1002/hyp.13786

Farid, A., Goodrich, D. C., Bryant, R., & Sorooshian, S. (2008). Using airborne lidar to predict Leaf Area Index in cottonwood trees and refine riparian water-use estimates. *Journal of Arid Environments*, *72*(1), 1–15. https://doi.org/10.1016/j.jaridenv.2007.04.010

Fraser, R. H., Olthof, I., Carrière, M., Deschamps, A., & Pouliot, D. (2011). Detecting long-term changes to vegetation in northern Canada using the Landsat satellite image archive. *Environmental Research Letters*, *6*(4). https://doi.org/10.1088/1748-9326/6/4/045502

Garner, G., Malcolm, I. A., Sadler, J. P., & Hannah, D. M. (2017). The role of riparian vegetation density , channel orientation and water velocity in determining river temperature dynamics. *Journal of Hydrology*, *553*, 471–485. https://doi.org/10.1016/j.jhydrol.2017.03.024

GDAL/OGR contributors (2019). GDAL/OGR Geospatial Data Abstraction software Library. Open Source Geospatial Foundation. URL https://gdal.org

Ghosh, A., Fassnacht, F. E., Joshi, P. K., & Kochb, B. (2014). A framework for mapping tree species combining hyperspectral and LiDAR data: Role of selected classifiers and sensor across three spatial scales. *International Journal of Applied Earth Observation and Geoinformation*, *26*(1), 49–63. https://doi.org/10.1016/j.jag.2013.05.017

Granger RJ. (1999). Partitioning of energy during the snow-free season at the Wolf Creek Research Basin. In Wolf Creek Research Basin: Hydrology, Ecology, Environment, Pomeroy JW, Granger RJ (eds). National Water Research Institute: Saskatoon; 55–78.

Greaves, H. E., Vierling, L. A., Eitel, J. U. H., Boelman, N. T., Magney, T. S., Prager, C. M., & Griffin, K. L. (2016). High-resolution mapping of aboveground shrub biomass in Arctic tundra using airborne lidar and imagery. *Remote Sensing of Environment*, *184*, 361–373. https://doi.org/10.1016/j.rse.2016.07.026

Guisan, A., Weiss, S. B., & Weiss, A. D. (1999). GLM versus CCA Spatial Modeling of Plant Species Distribution. *Plant Ecology*, *143*(1), 107–122. https://doi.org/10.1023/A:1009841519580

Harder, P., Schirmer, M., Pomeroy, J., & Helgason, W. (2016). Accuracy of snow depth estimation in mountain and prairie environments by an unmanned aerial vehicle. *Cryosphere*, *10*(6), 2559–2571. https://doi.org/10.5194/tc-10-2559-2016

Hengl, T., & Reuter, H. I. (2009). *Geomorphometry: Concepts, Software, Applications*. *Developments in Soil Science* (Volume 33, Vol. 33). Elsevier Science. https://doi.org/10.1016/S0166-2481(08)00012-3

Hinzman, L. D., Bettez, N. D., Bolton, W. R., Chapin, F. S., Dyurgerov, M. B., Fastie, C. L., … Yoshikawa, K. (2005). Evidence and implications of recent climate change in Northern Alaska and other Arctic regions. *Climatic Change*, *72*(3), 251–298. https://doi.org/10.1007/s10584-005-5352-2

Hopkinson, C., Chasmer, L. E., Sass, G., Creed, I. F., Sitar, M., Kalbfleisch, W., & Treitz, P. (2005). Vegetation class dependent errors in lidar ground elevation and canopy height estimates in a boreal wetland environment. *Canadian Journal of Remote Sensing*, *31*(2), 191–206. https://doi.org/10.5589/m05-007

Hopkinson, C., Chasmer, L., Lim, K., Treitz, P., & Creed, I. (2006). Towards a universal lidar canopy height indicator. *Canadian Journal of Remote Sensing*, *32*(2), 139–152. https://doi.org/10.5589/m06-006

Hopkinson, C., Chasmer, L., & Hall, R. J. (2008). The uncertainty in conifer plantation growth prediction from multi-temporal lidar datasets. *Remote Sensing of Environment*, *112*(3), 1168–1180. https://doi.org/10.1016/j.rse.2007.07.020

Hopkinson, C., & Chasmer, L. (2009). Testing LiDAR models of fractional cover across multiple forest ecozones. *Remote Sensing of Environment*, *113*(1), 275–288. https://doi.org/10.1016/j.rse.2008.09.012

Huang, C., Davis, L. S., & Townshend, J. R. G. (2002). An assessment of support vector machines for land cover classification. *International Journal of Remote Sensing*, *23*(4), 725–749. https://doi.org/10.1080/01431160110040323

Hyyppä, J., Hyyppä, H., Leckie, D., Gougeon, F., Yu, X., & Maltamo, M. (2008). Review of methods of small-footprint airborne laser scanning for extracting forest inventory data in boreal forests. *International Journal of Remote Sensing*, *29*(5), 1339–1366. https://doi.org/10.1080/01431160701736489

Isenburg, M. (2012). LASzip : lossless compression of LiDAR data. http://laszip.org

Isenburg, M. (2019). LAStools – efficient tools for LiDAR processing, Version 190927, http://lastools.org

Janowicz, J. R. (1999). Wolf Creek Research Basin - Overview. *Water Resources Division, Indian and Northern Affairs Canada*, 121–130.

Kellner, J. R., Armston, J., Birrer, M., Cushman, K. C., Duncanson, L., Eck, C., … Zgraggen, C. (2019). New Opportunities for Forest Remote Sensing Through Ultra-High-Density Drone Lidar. *Surveys in Geophysics*, *40*(4), 959–977. https://doi.org/10.1007/s10712-019-09529-9

Lafleur, P. M., & Humphreys, E. R. (2018). Tundra shrub effects on growing season energy and carbon dioxide exchange. *Environmental Research Letters*, *13*(5). https://doi.org/10.1088/1748-9326/aab863

Langley, S. K., Cheshire, H. M., & Humes, K. S. (2001). A comparison of single date and multitemporal satellite image classifications in a semi-arid grassland. *Journal of Arid Environments*, *49*(2), 401–411. https://doi.org/10.1006/jare.2000.0771

Lantz, T. C., Gergel, S. E., & Kokelj, S. V. (2010). Spatial Heterogeneity in the Shrub Tundra Ecotone in the Mackenzie Delta Region, Northwest Territories: Implications for Arctic Environmental Change. *Ecosystems*, *13*(2), 194–204. https://doi.org/10.1007/s10021-009-9310-0

Lawrence, D. M., & Swenson, S. C. (2011). Permafrost response to increasing Arctic shrub abundance depends on the relative influence of shrubs on local soil cooling versus large-scale climate warming. *Environmental Research Letters*, *6*(4). https://doi.org/10.1088/1748-9326/6/4/045504

Leckie, D. G., Gougeon, F. A., Tinis, S., Nelson, T., Burnett, C. N., & Paradine, D. (2005). Automated tree recognition in old growth conifer stands with high resolution digital imagery. *Remote Sensing of Environment*, *94*(3), 311–326. https://doi.org/10.1016/j.rse.2004.10.011

Lefsky, M. A., Cohen, W. B., Parker, G. G., & Harding, D. J. (2002). Lidar Remote Sensing for Ecosystem Studies. *BioScience*, *52*(1), 19. https://doi.org/10.1641/0006-3568(2002)052[0019:LRSFES]2.0.CO;2

Leutner, B., Horning, N., & Schwalb-Willmann, J. (2019). RStoolbox: Tools for Remote Sensing Data Analysis. R package version 0.2.6. https://CRAN.R-project.org/package=RStoolbox

Liaw, A., & Wiener, M. (2002). Classification and Regression by randomForest. *R News*, *2*(December), 18–22. https://doi.org/10.1177/154405910408300516

McCartney, S. E., Carey, S. K., & Pomeroy, J. W. (2006). Intra-basin variability of snowmelt water balance calculations in a subarctic catchment. *Hydrological Processes*, *20*(4), 1001–1016. https://doi.org/10.1002/hyp.6125

Ménard, C. B., Essery, R., & Pomeroy, J. (2014). Modelled sensitivity of the snow regime to topography, shrub fraction and shrub height. *Hydrology and Earth System Sciences*, *18*(6), 2375–2392. https://doi.org/10.5194/hess-18-2375-2014

Meyer, D., Dimitriadou, E., Hornik, K., Weingessel, A., & Leisch, F. (2019). e1071: Misc Functions of the Department of Statistics, Probability Theory Group (Formerly: E1071), TU Wien. R package version 1.7-3. https://CRAN.R-project.org/package=e1071

Millard, K., & Richardson, M. (2013). Wetland mapping with LiDAR derivatives, SAR polarimetric decompositions, and LiDAR-SAR fusion using a random forest classifier. *Canadian Journal of Remote Sensing*, *39*(4), 290–307. https://doi.org/10.5589/m13-038

Millard, K., & Richardson, M. (2015). On the importance of training data sample selection in Random Forest image classification: A case study in peatland ecosystem mapping. *Remote Sensing*, *7*(7), 8489–8515. https://doi.org/10.3390/rs70708489

Montealegre, A. L., Lamelas, M. T., & De La Riva, J. (2015). A Comparison of Open-Source LiDAR Filtering Algorithms in a Mediterranean Forest Environment. *IEEE Journal of Selected Topics in Applied Earth Observations and Remote Sensing*, *8*(8), 4072–4085. https://doi.org/10.1109/JSTARS.2015.2436974

Myers-Smith, I. H., Forbes, B. C., Wilmking, M., Hallinger, M., Lantz, T., Blok, D., … Hik, D. S. (2011). Shrub expansion in tundra ecosystems: Dynamics, impacts and research priorities. *Environmental Research Letters*, *6*(4). https://doi.org/10.1088/1748-9326/6/4/045509

Myers-Smith, I. H., & Hik, D. S. (2018). Climate warming as a driver of tundra shrubline advance. *Journal of Ecology*, *106*(2), 547–560. https://doi.org/10.1111/1365-2745.12817

Næsset, E. (2004). Effects of different flying altitudes on biophysical stand properties estimated from canopy height and density measured with a small-footprint airborne scanning laser. *Remote Sensing of Environment*, *91*(2), 243–255. https://doi.org/10.1016/j.rse.2004.03.009

Næsset, E. (2009). Effects of different sensors, flying altitudes, and pulse repetition frequencies on forest canopy metrics and biophysical stand properties derived from small-footprint airborne laser data. *Remote Sensing of Environment*, *113*(1), 148–159. https://doi.org/10.1016/j.rse.2008.09.001

Naito, A. T., & Cairns, D. M. (2011). Relationships between Arctic shrub dynamics and topographically derived hydrologic characteristics. *Environmental Research Letters*, *6*(4). https://doi.org/10.1088/1748-9326/6/4/045506

Naito, A. T., & Cairns, D. M. (2011). Patterns and processes of global shrub expansion. *Progress in Physical Geography*, *35*(4), 423–442. https://doi.org/10.1177/0309133311403538

Naito, A. T., & Cairns, D. M. (2015). Patterns of shrub expansion in Alaskan arctic river corridors suggest phase transition. *Ecology and Evolution*, *5*(1), 87–101. https://doi.org/10.1002/ece3.1341

Nichols, W. F., Killingbeck, K. T., & August, P. V. (2008). The Influence of Geomorphological Heterogeneity on Biodiversity II. A Landscape Perspective. *Conservation Biology*, *12*(2), 363–370. https://doi.org/10.1111/j.1523-1739.1998.96238.x

Overpeck, J., Hughen, K., Hardy, D., Bradley, R., Case, R., Douglas, M., … Zielinski, G. (1997). Arctic environmental change of the last four centuries. *Science*, *278*(5341), 1251–1256. https://doi.org/10.1126/science.278.5341.1251

PDAL Contributors. (2019). PDAL Point Data Abstraction Library. doi:10.5281/zenodo.2556738

Pearson, R. G., Phillips, S. J., Loranty, M. M., Beck, P. S. A., Damoulas, T., Knight, S. J., & Goetz, S. J. (2013). Shifts in Arctic vegetation and associated feedbacks under climate change. *Nature Climate Change*, *3*(7), 673–677. https://doi.org/10.1038/nclimate1858

Piovano, T. I., Tetzlaff, D., Carey, S. K., Shatilla, N. J., Smith, A., & Soulsby, C. (2019). Spatially distributed tracer-aided runoff modelling and dynamics of storage and water ages in a permafrost-influenced catchment. *Hydrology and Earth System Sciences*, *23*(6), 2507–2523. https://doi.org/10.5194/hess-23-2507-2019

Pohl, S., Marsh, P., & Bonsal, B. R. (2007). Modeling the impact of climate change on runoff and annual water balance of an arctic headwater basin. *Arctic*, *60*(2), 173–186. https://doi.org/10.14430/arctic242

Pomeroy, J. W., Bewley, D. S., Essery, R. L. H., Hedstrom, N. R., Link, T., Granger, R. J., … Janowicz, J. R. (2006). Shrub tundra snowmelt. *Hydrological Processes*, *20*(4), 923–941. https://doi.org/10.1002/hyp.6124

R Core Team (2019). R: A language and environment for statistical computing. R Foundation for Statistical Computing, Vienna, Austria. URL https://www.R-project.org/.

Rasouli, K., Pomeroy, J. W., Janowicz, J. R., Williams, T. J., & Carey, S. K. (2019). A long-term hydrometeorological dataset (1993-2014) of a northern mountain basin: Wolf Creek Research Basin, Yukon Territory, Canada. *Earth System Science Data*, *11*(1), 89–100. https://doi.org/10.5194/essd-11-89-2019

Richards, J. A. (2013). Remote Sensing Digital Image Analysis. *Springer Heidelberg*. https://doi.org/10.1007/978-3-642-30062-2

Roussel, J. R., Caspersen, J., Béland, M., Thomas, S., & Achim, A. (2017). Removing bias from LiDAR-based estimates of canopy height: Accounting for the effects of pulse density and footprint size. *Remote Sensing of Environment*, *198*, 1–16. https://doi.org/10.1016/j.rse.2017.05.032

Roussel, J.R. & Auty, D. (2019). lidR: Airborne LiDAR Data Manipulation and Visualization for Forestry Applications. R package version 2.1.2. https://CRAN.R-project.org/package=lidR

Shatilla, N. J., & Carey, S. K. (2019). Assessing inter-annual and seasonal patterns of DOC and DOM quality across a complex alpine watershed underlain by discontinuous permafrost in Yukon, Canada. *Hydrology and Earth System Sciences*, *23*(9), 3571–3591. https://doi.org/10.5194/hess-23-3571-2019

Smeeckaert, J., Mallet, C., David, N., Chehata, N., & Ferraz, A. (2013). Large-scale classification of water areas using airborne topographic lidar data. *Remote Sensing of Environment*, *138*, 134–148. https://doi.org/10.1016/j.rse.2013.07.004

de Smith, M. J., Goodchild, M. F., Longley P. A., & Associates (2018). Geospatial Analysis: A Comprehensive Guide to Principles Techniques and Software Tools, 6th Edition. https://spatialanalysisonline.com/

Sørensen, R., Zinko, U., & Seibert, J. (2006). On the calculation of the topographic wetness index: Evaluation of different methods based on field observations. *Hydrology and Earth System Sciences*, *10*(1), 101–112. https://doi.org/10.5194/hess-10-101-2006

Sothe, C., De Almeida, C. M., Schimalski, M. B., Liesenberg, V., La Rosa, L. E. C., Castro, J. D. B., & Feitosa, R. Q. (2020). A comparison of machine and deep-learning algorithms applied to multisource data for a subtropical forest area classification. *International Journal of Remote Sensing*, *41*(5), 1943–1969. https://doi.org/10.1080/01431161.2019.1681600

Streutker, D. R., & Glenn, N. F. (2006). LiDAR measurement of sagebrush steppe vegetation heights. *Remote Sensing of Environment*, *102*(1–2), 135–145. https://doi.org/10.1016/j.rse.2006.02.011

Sturm, M., Racine, C., & Tape, K. (2001). Increasing shrub abundance in the Arctic. *Nature*, *411*(6837), 546–547. https://doi.org/10.1038/35079180

Sturm, M., Holmgren, J., McFadden, J. P., Liston, G. E., Chapin, F. S., & Racine, C. H. (2001). Snow–Shrub Interactions in Arctic Tundra: A Hypothesis with Climatic Implications. *Journal of Climate*, *14*(3), 336–344. https://doi.org/10.1175/1520-0442(2001)014<0336:SSIIAT>2.0.CO;2

Tape, K., Sturm, M., & Racine, C. (2006). The evidence for shrub expansion in Northern Alaska and the Pan-Arctic. *Global Change Biology*, *1*(2), 686–702. https://doi.org/10.1111/j.1365-2486.2006.01128.x

Tape, K. D., Verbyla, D., & Welker, J. M. (2011). Twentieth century erosion in Arctic Alaska foothills: The influence of shrubs, runoff, and permafrost. *Journal of Geophysical Research: Biogeosciences*, *116*(4), 1–11. https://doi.org/10.1029/2011JG001795

Tape, K. D., Hallinger, M., Welker, J. M., & Ruess, R. W. (2012). Landscape Heterogeneity of Shrub Expansion in Arctic Alaska. *Ecosystems*, *15*(5), 711–724. https://doi.org/10.1007/s10021-012-9540-4

Tétreault, P., Kouba, J., Héroux, P., & Legree, P. (2005). CSRS-PPP: An internet service for GPS user access to the Canadian Spatial Reference Frame. *Geomatica*, *59*(1), 17-28.

Tetzlaff, D., Soulsby, C., Buttle, J., Capell, R., Carey, S. K., Laudon, H., … Shanley, J. (2013). Catchments on the cusp? Structural and functional change in northern ecohydrology. *Hydrological Processes*, *27*(5), 766–774. https://doi.org/10.1002/hyp.9700

Tremblay, B., Lévesque, E., & Boudreau, S. (2012). Recent expansion of erect shrubs in the Low Arctic: Evidence from Eastern Nunavik. *Environmental Research Letters*, *7*(3). https://doi.org/10.1088/1748-9326/7/3/035501

Ussyshkin, RV., Smith, B., Fidera, A. (2006). Performance Evaluation of Optech's ALTM 3100: Study of Georeferencing Accuracy. *ION TM*.

Ussyshkin, V., & Theriault, L. (2011). Airborne lidar: Advances in discrete return technology for 3D vegetation mapping. *Remote Sensing*, *3*(3), 416–434. https://doi.org/10.3390/rs3030416

Véronneau, M., Mainville, A., & Craymer, M. R. (2001). The GPS height transformation (v2. 0): An ellipsoidal-CGVD28 height transformation for use with GPS in Canada. Report, Geodetic Survey Division, Earth Sciences Sector. Natural Resources Canada, Ottawa.

Walker, D. A., Jia, G. J., Epstein, H. E., Raynolds, M. K., Chapin, I. S., Copass, C., … Shiklomanov, N. (2003). Vegetation-soil-thaw-depth relationships along a low-arctic bioclimate gradient, Alaska: Synthesis of information from the ATLAS studies. *Permafrost and Periglacial Processes*, *14*(2), 103–123. https://doi.org/10.1002/ppp.452

Wallace, C. A., & Baltzer, J. L. (2019). Tall Shrubs Mediate Abiotic Conditions and Plant Communities at the Taiga–Tundra Ecotone. *Ecosystems*. https://doi.org/10.1007/s10021-019-00435-0

Wehr, A., & Lohr, U. (1999). Airborne laser scanning—an introduction and overview. *ISPRS Journal of Photogrammetry and Remote Sensing*, *54*(2–3), 68–82. https://doi.org/10.1016/S0924-2716(99)00011-8

Wilson, J. P. & Gallant, J. C. (2000). Terrain Analysis: Principles and Applications. *New York, © John Wiley & Sons, Inc.*

Wu, X. Ben, & Archer, S. R. (2005). Scale-dependent influence of topography-based hydrologic features on patterns of woody plant encroachment in savanna landscapes. *Landscape Ecology*, *20*(6), 733–742. https://doi.org/10.1007/s10980-005-0996-x

Wu, B., Yu, B., Wu, Q., Huang, Y., Chen, Z., & Wu, J. (2016). Individual tree crown delineation using localized contour tree method and airborne LiDAR data in coniferous forests. *International Journal of Applied Earth Observation and Geoinformation*, *52*, 82–94. https://doi.org/10.1016/j.jag.2016.06.003

Zhang, K., Chen, S. C., Whitman, D., Shyu, M. L., Yan, J., & Zhang, C. (2003). A progressive morphological filter for removing nonground measurements from airborne LIDAR data. *IEEE Transactions on Geoscience and Remote Sensing*, *41*(4 PART I), 872–882. https://doi.org/10.1109/TGRS.2003.810682

Zhang, W., Qi, J., Wan, P., Wang, H., Xie, D., Wang, X., & Yan, G. (2016). An easy-to-use airborne LiDAR data filtering method based on cloth simulation. *Remote Sensing*, *8*(6), 1–22. https://doi.org/10.3390/rs8060501

Zhao, K., Suarez, J. C., Garcia, M., Hu, T., Wang, C., & Londo, A. (2018). Utility of multitemporal lidar for forest and carbon monitoring: Tree growth, biomass dynamics, and carbon flux. *Remote Sensing of Environment*, *204*(September 2016), 883–897. https://doi.org/10.1016/j.rse.2017.09.007

Zwieback, S., Chang, Q., Marsh, P., & Berg, A. (2019). Shrub tundra ecohydrology: Rainfall interception is a major component of the water balance. *Environmental Research Letters*, *14*(5). https://doi.org/10.1088/1748-9326/ab1049

APPENDIX

Table A.1: Rasterized 1 m resolution DEM height errors vs. dGPS position (m) over different land cover types created using the original 2018, thinned 2018, and 2007 point clouds.

	2007		**2018 (Original)**		**2018 (Thinned)**	
	Roads	Vegetation	Roads	Vegetation	Roads	Vegetation
Last-returns						
Avg	-0.07	0.13	0.05	0.28	0.07	0.11
AvgAbs	0.10	0.26	0.06	0.29	0.09	0.17
Min	-0.55	-0.64	-0.17	-0.39	-0.13	-0.51
Max	0.37	1.90	0.26	1.87	0.56	1.15
SD	0.09	0.40	0.06	0.31	0.09	0.21
RMSE	0.12	0.42	0.08	0.41	0.12	0.23
Ground returns						
Avg	-0.15	-0.19	-0.01	-0.08	0.07	0.13
AvgAbs	0.17	0.23	0.05	0.15	0.09	0.19
Min	-0.77	-0.10	-0.42	-1.18	-0.13	-0.51
Max	0.21	0.39	0.21	0.34	0.55	1.43
SD	0.16	0.21	0.06	0.20	0.09	0.23
RMSE	0.22	0.28	0.06	0.22	0.12	0.29

Table A.2: Field-measured vegetation heights (in m) from transect surveys: original point measurements (9x per plot), averaged per 1 m radius plot, and highest per plot

	Vegetation class				
	All plots	All shrubs	Willow	Birch	Grass/moss
All point measures					
Avg	0.87	1.09	1.24	0.69	0.15
Min	0	0	0	0.06	0
Max	3.70	3.70	3.70	1.75	1.70
SD	0.69	0.63	0.65	0.34	0.19
N	1284	981	711	238	303
Average plot height					
Avg	0.85	0.88	0.94	0.62	0.15
Min	0.06	0.06	0.06	0.11	0.11
Max	3.22	3.22	3.22	1.34	0.18
SD	0.55	0.55	0.58	0.30	0.04
N	145	142	114	27	3
Maximum plot height					
Avg	1.41	1.43	1.51	1.11	0.27
Min	0.18	0.18	0.18	0.22	0.20
Max	3.70	3.70	3.70	1.83	0.36
SD	0.62	0.61	0.63	0.40	0.08

Table A.3: Maximum LAS return heights within 1 m radius field survey plots from 2018 original, 2018 thinned, and 2007 point clouds

	Vegetation class				
	All plots	All shrubs	Willow	Birch	Grass/moss
2018 Original ($11.9/m^2$)					
Avg	1.29	1.29	1.36	0.97	0.20
Min	0.08	0.08	0.16	0.08	0.10
Max	3.56	3.56	3.56	2.12	0.34
SD	0.65	0.64	0.64	0.51	0.12
N	145	142	114	27	3
2018 Thinned ($0.67/ m^2$)					
Avg	0.52	0.53	0.59	0.27	0.06
Min	0	0	0	0	0
Max	3.07	3.07	3.07	1.78	0.10
SD	0.71	0.71	0.75	0.46	0.53
N	138	135	108	26	3
2007 ($0.67/m^2$)					
Avg	0.25	0.25	0.28	0.08	0.06
Min	0	0	0	0	0
Max	2.23	2.23	2.23	0.53	0.18
SD	0.41	0.41	0.44	0.14	0.10
N	139	136	108	27	3

Table A.4: Summary statistics for all accuracies and shrubbed areas over 25 different seed iterations for the random forests and support vector machines classifiers

	Producer's (Absence)	User's (Absence)	Producer's (Presence)	Producer's (Absence)	Overall Accuracy	Cohen's kappa	Shrubbed Area (km^2)
Random Forests							
mean	98.95	88.98	87.18	98.64	93.12	0.86	1.55
std	2.55	4.41	5.94	3.58	2.81	0.06	0.10
min	88.10	79.07	73.53	82.76	86.76	0.74	1.42
max	100	96.88	97.22	100	97.06	0.94	1.93
range	11.90	17.81	23.69	17.24	10.29	0.21	0.51
Support Vector Machines							
mean	99.09	88.22	86.27	98.76	92.71	0.85	1.45
std	2.81	4.43	5.79	3.99	2.83	0.06	0.15
min	88.10	79.07	73.53	82.76	86.76	0.74	1.32
max	100	96.97	97.22	100	98.53	0.97	1.94
range	11.90	17.90	23.69	17.24	11.76	0.24	0.63